MEASUREMENTS OF CONTINUOUS ENERGY DISTRIBUTIONS OF GAMMA RAYS IN A SCATTERING MEDIUM

PROEFSCHRIFT

TER VERKRIJGING VAN DE GRAAD VAN DOCTOR IN DE TECHNISCHE WETENSCHAP AAN DE TECHNISCHE HOGESCHOOL TE DELFT OP GEZAG VAN DE RECTOR MAGNIFICUS DR R. KRONIG, HOOGLERAAR IN DE AFDELING DER TECHNISCHE NATUURKUNDE, VOOR EEN COMMISSIE UIT DE SENAAT TE VERDEDIGEN OP WOENSDAG 27 SEPTEMBER 1961 DES NAMIDDAGS TE 2 UUR

DOOR

CHRISTIAAN SYBESMA
NATUURKUNDIG INGENIEUR

GEBOREN TE BANDOENG

Dit proefschrift is goedgekeurd door de promotor

PROF. DR J. J. WENT

Voor Chrisje en Babette

Het onderzoek, beschreven in dit proefschrift, werd verricht in het Laboratorium van de Afdeling Stofwisselingsziekten en Endocrinologie (hoofd: PROF. DR. A. QUERIDO) van het Academisch Ziekenhuis te Leiden.

Financiële steun voor dit onderzoek werd verleend door het Instituut voor Radiopathologie en Stralenbescherming te Leiden. De heren J. VAN ZIJL en J. J. BREGONJE, beiden in dienst van dit Instituut, waren bij de experimenten behulpzaam.

Met DRS. HUB. WIJKER mocht schrijver een aantal zeer vruchtbare discussies hebben.

Het inverteren van de matrices en het oplossen van de stelsels vergelijkingen werd onder leiding van DR. TH. J. DEKKER uitgevoerd met de digitale rekenautomaat X–1 van de Rekenafdeling van het Mathematisch Centrum te Amsterdam.

Contents

Introduction

The still increasing use of more or less extensive radioactive sources in numerous applications has rendered penetration and attenuation of gamma and X-rays a problem of increasing importance. This may be obvious, for example, in designing shielding facilities for nuclear reactor plants. However, also in the applications of ionizing radiation in medicine these penetration problems are extremely important.

To illustrate the nature and the difficulties of the penetration problems, we consider a point source, emitting monoenergetic gamma rays in vacuum, with a detector at a certain distance from the source and a disk of some material with a thickness x, placed between the source and the detector. If the gamma rays are collimated in such a way that only gamma rays that are incident along the joining line between the source and the detector are counted, the reading of the detector is decreased with a factor $e^{\mu x}$, in which μ is the attenuation coefficient of the material involved at the photon energy of the source. Such an arrangement is known as a 'good geometry' configuration. An example of a 'bad geometry' configuration is present when there is no collimation at all. In that case photons which are scattered somewhere in the disk can also enter the detector. Other examples of 'bad geometry' configurations are a source and a detector immersed within a scattering medium, a source outside the medium and a detector immersed within the medium, and an immersed source and an external detector. In all these cases of 'bad geometry' the attenuation factor, mentioned above, must be corrected for the effect of multiple scattered photons.

'Bad geometry' configurations are found in the majority of the applications of ionizing radiation. An outstanding example of such a 'bad geometry' in medical applications is the geometry encountered in the telecurie and X-ray therapy. As the depth dose in tissue is greatly influenced by multiple scatter effects, depth dose values, measured in phantoms (Morgan 1954) show appreciable differences with the dose, calculated according to the mentioned 'good geometry' attenuation (see fig. 1). Another example in medical applications is the dose delivered to

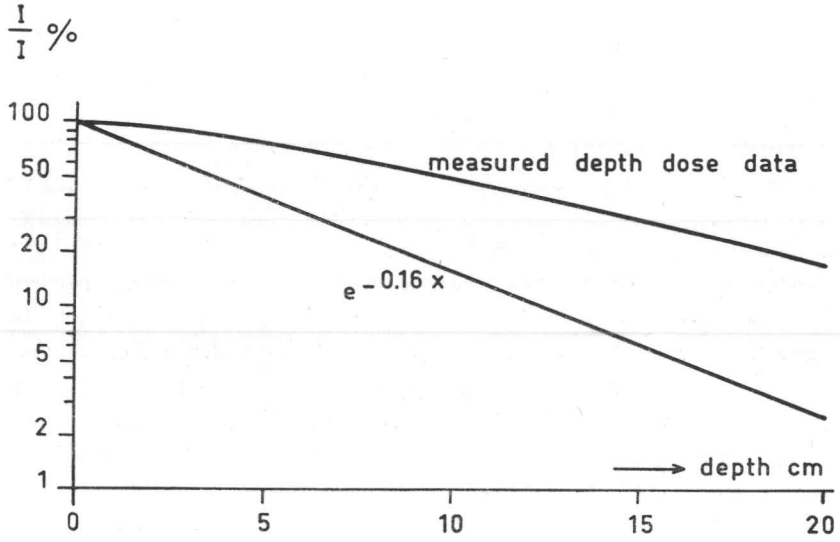

Fig. 1. Measured procentual depth dose data compared with 'good geometry' attenuation in soft tissue.

the tissue by radium or cobalt applicators. These applicators are characterized by isodose curves, which are measured in air. The dose 'delivered to the tissue' is usually taken from these curves. While this could be done relatively safely at distances not exceeding 2 or 3 cm, at greater distances the discrepancy between those values and the true dose increases rapidly.

As the importance of multiple scattering in penetration problems is now highly appreciated, considerable effort has been devoted to find data about the intensity and the energy distributions of photons, which are scattered when gamma and X-rays are penetrating a medium. However, though to this purpose calculations of various degrees of rigour have been elaborated, experimental data to check these calculations are still scanty. Some measurements of dose buildup factors (Garret *et al*, 1954; White, 1954; Mellink, 1954, 1957) are in reasonable agreement with theoretically predicted values. Direct measurements of energy distributions with the aid of scintillation spectrometry, however, still meet with difficulties. Due to these difficulties, the few results known until now (Bruce *et al*, 1955; Hayward, 1952; Theus *et al*, 1955) include more or less serious uncertainties.

These difficulties arise mainly in the interpretation of the measured pulse height spectra. Since not all of the incident photon energy is absorbed in the scintillating material, corrections have to be made for the occurring escape effects (which may be complicated by interactions in the scintillating material). Moreover, a pulse height spectrum is 'smeared out' as a result of the statistical processes in the scintillation detector. This 'smearing out' causes large mathematical difficulties in determining continuous photon energy distributions from measured pulse height spectra.

In the work described in this thesis an attempt is made to overcome all these difficulties. The following chapters deal with measurements of continuous photon energy distributions, resulting from scattering of gamma rays in a water medium, with the aid of a single channel scintillation spectrometer. The geometry chosen was such that the measuring conditions were comparable with conditions found in radiological applications (*i.e.* a point isotropic source approximately in the centre of a bounded water medium). With this geometry comparison with calculations according to the 'moment method' of Spencer and Fano (1951) is possible, as Berger *et al* (1959) have shown.

To induce the scatter effects ^{60}Co may be considered, this nuclide being widely used in radiological applications. However, the fact that the gamma radiation of ^{60}Co comprises photons of two different energies (*i.e.* 1.17 MeV and 1.33 MeV) enlarges the difficulties in the correction of the measured pulse height spectra. Therefore ^{137}Cs was chosen for this purpose, this nuclide emitting monoenergetic gamma rays with an energy of 0,66 MeV.

Measurements of pulse height distributions in such a bounded water medium are described in chapter II, a general formulation of the penetration problems and a summary of publications on this subject being given in chapter I. The difficulties in the correction of the measured pulse height distributions are discussed in chapter III. In chapter IV a solution of the problems concerning the spread in the pulse height is proposed, while in chapter V the correction of the energy escape effects in the scintillation crystal is discussed. These corrections are applied to the pulse height distribution measurements described in chapter II, the resulting photon energy distributions and buildup factors being discussed in chapter VI. Finally, in chapter VII, the possibility of applying the described measuring and correction method to measurements with other geometries is discussed, one of these geometries being described in more detail.

CHAPTER I

Multiple scattering of gamma and X-rays

1. TYPES OF INTERACTION

Different types of interaction of photons with matter contribute to the angular energy distributions within, and in the neighbourhood of, a scattering medium. It may be convenient to give a brief summary of the possible types of interaction, and the mode at which they contribute to the angular energy distributions.

In the penetration of gamma rays through a medium, the following interaction processes between photons and matter are possible:

a. Coherent (Rayleigh) scattering
b. Atomic photoelectric effect
c. Compton scattering
d. Pair production
e. Nuclear scattering
f. Nuclear interactions

Secondary processes arising out of these interactions are:

g. Fluorescence radiation
h. Bremsstrahlung
i. Annihilation radiation

The processes e. and f. can be dismissed immediately, since below 10 MeV these are not likely to occur.

Rayleigh scattering, as it is coherent, does not involve energy losses but only small (Fano, 1953) angle deflections, and, accordingly, affects only the angular distributions. In all methods for calculating the intensity and the energy distributions of scattered photons, this coherent scattering is neglected. This certainly is justified in the case of low Z materials, since the coherent scattering cross section for low Z materials is only a small fraction of the incoherent compton scattering cross section (Goldstein, 1954). Though coherent scattering increases much more rapidly with Z than does the incoherent scattering, the neglection can be done without much danger even for high Z materials, since for elements with

higher atomic number the photoelectric cross section increases so much more rapidly than does the coherent scattering cross section, that the latter is an ever decreasing fraction of the total attenuation cross section. Moreover, for higher energies (above 0.5 MeV) even the highly bound electrons appear free, so that for these energies incoherent compton scattering is the dominant process.

The secondary processes are not likely to influence the energy distributions to a great extent. The energy of fluorescence radiation (X-radiation following photoelectric effect) is too low to be of great influence except in the very heavy elements. Bremsstrahlung, arising from compton recoil electrons and pair produced electrons is not very likely with source energies below 10 MeV (see table I of ref. Foldi 1951). Appreciable annihilation radiation only occurs with very high energy sources where pair production becomes important. Pair production only occurs at energies larger than 1.02 MeV, the energy equivalent of one electron pair.

Accordingly in an energy range between 0 and 0.66 MeV, as considered here, only the processes b. and c. are to be regarded; of these processes the atomic photoelectric effect is purely absorptive and the compton scattering is the one which gives rise to the spectrum of degraded photons.

2. MATHEMATICAL FORMULATION OF THE INTERACTION RESULTS

The angular energy distribution resulting from these processes can be represented by a function $N(\mathbf{r},\mathbf{u},E)$, such that

$$N(\mathbf{r},\mathbf{u},E)\,dudE$$

is the number of photons, of energy E in the range dE, and moving in the direction of the unit vector $\mathbf{u}$ in the element of solid angle du, which cross in unit time through a unit area located at the point $\mathbf{r}$ whose normal is in the direction $\mathbf{u}$.

The angular energy distribution function $N(\mathbf{r},\mathbf{u},E)$ is determined in general bij six variables, three of position $\mathbf{r}$, two of direction $\mathbf{u}$, and one of energy E. The Boltzmann transport equation, which is the equation of continuity in a photon phase space consisting of the six variables, can be derived, considering equilibrium state in a differential volume in phase space $dVdudE$. In cases of simplified source geometries the number of variables can be reduced to three. For example for a point isotropic source in a homogeneous medium, N is a function of r (the radial distance

from the source), φ (the angle between the radius vector and the photon direction) and E (the energy).

With a receiver of gamma rays which can discriminate in energy but which is insensitive to the angle at which the photons arrive (*i.e.* an isotropic receiver) the measurable quantity is not the angular energy distribution function N but the energy spectrum:

$$S(\mathbf{r},E) = \int_{4\pi} N(\mathbf{r},\mathbf{u},E)du \tag{I-1}$$

As most of the gamma ray receivers of interest, such as ionization chambers, scintillation detectors, volume elements of tissue, homogeneous shields and the like are approximately isotropic, the interesting quantity is the energy spectrum S (or the energy flux I, given by $IdE = ESdE$, which quantity is important in connection with ionization chambers and biological dosimetry problems), rather than the angular energy distribution function N.

The energy spectrum S, as well as all other functions of photon movement can be written as the sum of two components:

$$S = S_0 + S_s \tag{I-2}$$

in which the subscript 0 denotes those photons which have suffered no collision at all, and the subscript s those which have made at least one collision.

The unscattered component, for example S_0 in equation I–2, can usually be obtained quite simply. The scattered component is very difficult to calculate. Although the contribution of once scattered photons to the scattered component can be calculated without too many difficulties, it is extremely difficult to determine, without making any approximation, the contribution of those photons which have suffered more than one collision.

In penetration problems a convenient way to account for scatter complications is the use of buildup factors. In the majority of gamma ray measuring instruments, especially those in radiological applications, the gamma ray detectors are not able to measure the energy spectrum directly, *i.e.* to separate the contribution of scattered and unscattered photons. Their response is to some sort of average of the energy spectrum, which average is different for each type of detector. To account for these discre-

pancies one can define a multiplicative factor, a so called buildup factor, with which the response of the detector to the unscattered component must be multiplied to yield the actual instrument reading. Obviously a buildup factor varies not only with the type of detector used but also with the material present in the medium and with the distance from the source, the latter because of changes in the angular energy distributions. Goldstein and Wilkins (1954) offer the following, more generalized, formal definition of the buildup factor.

Suppose D is some linear operator working upon the angular distribution function N. Then DN can be splitted in two components, similar to those defined in equation (I–2):

$$DN = DN_0 + DN_s \tag{I–3}$$

When DN_0 is non vanishing, the buildup factor with respect to the operator D, B_D, is defined by the relation

$$DN = B_D DN_0 \tag{I–4}$$

As an example of this definition we consider the total number of photons incident on a unit differential volume, $S(\mathbf{r},E)dE$. The operator corresponding to this function is

$$D_N(\ ) = \int dudE(\ ) \tag{I–5}$$

and according to the equations I–3 and I–4, the associated buildup factor, the number buildup factor, is given by

$$B_N = \frac{\int S\,dE}{\int S_0 dE} \tag{I–6}$$

Similarly one can define other buildup factors, such as the dose buildup factor, the energy absorption buildup factor etc. While other types of buildup factors are possible, the most common buildup factors, as defined in this section, are of the type in which the operator has the form $D(\ ) = \int f(E)dudE(\ )$, with buildup factors

$$B_f = \frac{\int f(E)S(E)dE}{\int f(E)S_0(E)dE} \tag{I–7}$$

The calculation of any buildup factor of the type defined by equation (I–7) can be made if the function $S(E)$ is known, either by calculation or by measurement. It should be emphasized however, that the buildup factor is useful only in problems concerning the transmission of gamma rays and is essentially meaningless in situations in which the unscattered component vanishes, *i.e.* in backscatter or reflection problems.

3. CALCULATIONS AND MEASUREMENTS ON THE PENETRATION OF GAMMA AND X-RAYS

In the radiological field a few attempts have been made by radiologists to calculate and measure scatter effects in living tissue. In 1937 Payne-Scott calculated the contribution of the single scattered radiation to the depth dose. Lamerton (1948), using these calculations and those of R. de Waard (1946), estimated the influence of multiple scattering by employing the true absorption coefficient instead of the total attenuation coefficient. Experimental verification showed that the results of these calculations are too low for soft radiation and fit fairly well to much harder radiation (X-rays of 10 mmCu HCL). Calculations have also been made for the gamma radiation of ^{60}Co. Measurements in phantoms, carried out by Mellink (1954, 1957) were in good agreement with these calculations. In 1958 Schaal, investigating scatter effects of diagnostic X-rays in phantoms, measured changes in the half value layers due to scattering. Spectral distributions of radiation, scattered within a kilocurie ^{60}Co unit were measured by Cormack *et al* (1958).

Since the use of more intense sources of gamma rays is increased enormously during the past decade, problems concerned to deep penetrations of gamma rays now are considered more fundamentally. Peebles (1953) derivated a recurrence formula, giving the relation between the probability of transmission of a photon through a finite slab of material after $k + 1$ collisions and the same transmission probability after k collisions. This formula is based upon the assumption that a photon 'has lost its memory' of the foregoing interaction events in the material. The accuracy is estimated to be not better than 20%. This also is the case with the analytic approach of Maignan (1953) to the penetration problem. Estimating the radiation intensity at a distance r from a point source in a scattering medium with spherical symmetry, Maignan made an approximate calculation of the second and higher order scattered component, using an

average energy and average angle instead of the true energy and angular spectrum that is subject to second and higher order scattering. The results of these calculations, compared with measurements with a Geiger-Muller tube are quite satisfactory. However, the energy dependency of the counting tube still makes the comparison somewhat doubtful.

A calculation method on a purely numerical base is the random sampling or 'Monte Carlo' method, which can be applied on automatic computors. This method can be used for solving various types of problems. Several authors have used this method in solving a diversity of problems (Berger, 1955, 1956, 1957, 1960; Dixon, 1958; Perkins, 1955). However, the time consuming character of the computations is a serious limitation to the application of this method.

O'Rourke (1952, 1953) developed solution methods for the transport equation in finite and semi-infinite plane parallel media on a semi-numerical base. The numerical elaboration of these methods, however, is very complicated.

A semi-numerical method, which probably can be considered as the most important one for calculating the scattered photon energy distributions and the buildup factors, is the so called 'moment method', introduced by Spencer and Fano (1951). This moment method reduces the Boltzmann transport equation in an infinite homogeneous medium to a set of interlinked integral equations with the energy (the wavelength) as the independent variable. These equations can be solved numerically for the spatial moments of the angular energy distribution function N. An approximate determination of N should be possible from the knowledge of only a few of its moments. This method is suitable for high speed automatic calculation. Goldstein and Wilkins (1954) have carried out this procedure and calculated energy distributions and buildup factors for a large number of media and initial photon energies on the SEAC automatic computor of the American National Bureau of Standards. The inaccuracy of these calculations is believed not to exceed 5% in general.

The applicability of this method is limited to infinite homogeneous media. However, Berger *et al* (1959) clearly demonstrated that there are no great differences between calculations according to this method and 'Monte Carlo' calculations for bounded media. The energy dissipation near a spherical boundary, calculated according to the 'Monte Carlo' method for a 1.25 MeV gamma ray source in the centre, and compared with calculations according to the 'moment method' shows differences up to 14% but in general much smaller.

It is useful to compare these more or less theoretical treatments with experiments on the penetration of gamma rays in different materials. Such experiments on the penetration of gamma and X-rays can be distinguished in three groups:

a. measurements of buildup factors;
b. measurements of electron energy distributions in the penetrated medium;
c. direct measurements of scattered photon energy distributions.

Dose buildup factors could be measured with reasonable accuracy with the aid of an air equivalent walled ionization chamber. Such was done by Garret and Whyte (1954) for iron and lead using the gamma radiation of ^{60}Co, and by White (1954) for water also using the gamma radiation of ^{60}Co. In both cases the differences between theoretically predicted values and the results of the measurements do not exceed 5%. Garret and Whyte have shown that the discrepancies between theory and experiments could be explained by inaccuracies in the used absorption coefficients.

Measurements of group b have been carried out by Bruce and Johns (1955) and by Hayward (1952). Bruce *et al* and Hayward measured the electron energy distribution resulting from respectively an external beam of ^{60}Co gamma radiation incident on water (monodirectional plane source), and a point isotropic ^{60}Co source in water. In both cases the energy distribution of electrons produced in an anthracene crystal immersed in water was measured. Limitations of this method, indicated by the authors, are the poor resolution of the detector and the fact that electrons produced outside the crystal and scattered into the same, as well as electrons produced inside the crystal and scattered out of the same, are incorrectly detected. The amount of the latter effect of course is dependent on the size of the crystal. However, using a larger crystal the probability of 'pile up' in the crystal is increased. Another limitation, which is not indicated, is the non linear response of an anthracene scintillation crystal to electrons with energy below 0.12 MeV (Taylor *et al*, 1951).

The only measurements in group c, so far known, are those of Theus, Beach and Faust (1955). The method used by these authors involved a more rigorous analysis of pulse height spectra arising from scattering of ^{137}Cs gamma rays in water. The detector was a thallium activated sodium iodide crystal mounted on a photomultiplier which was connected to a twenty channel pulse height analyser. The response of the detector to

incident photons in a continuous range of energies can be expressed in a response equation, which is an integral equation of the first kind (Whittaker and Watson, 1952). The kernel of this equation is non symmetric and is greatly determined by an exponential function which described the statistical 'smearing out' by the detector. To perform the inversion of the integral equation the authors expressed the latter as the limit, $m \to \infty$ of a matrix equation. This matrix equation should be approximately solvable by the use of a finite value of m. According to Dixon and Aitken (1958) a difficulty of this approach to the solution is that the determinant of the matrix to be inversed probably tends to become zero in the limit case, due to the experimental function in the transformed kernel. In that case the matrix inversion should be mathematically invalid.

There are some other uncertainties in the method of Theus *et al* which make their results somewhat doubtful. The most important of these uncertainties is the neglection of secondary interactions in the crystal. As will be seen later in this thesis these secondary interactions are not fully taken account of by experimentally determining the relative photo-electric and compton probability. There are reasons to believe that the discrepancies found by Theus *et al* between the energy buildup factor calculated according to Goldstein *et al* (1954) and the experimentally determined energy buildup factors (20% and more) are mainly caused by these incertainties.

More careful measurements and a refined discussion of their value are therefore highly desirable.

CHAPTER II

Measurements of pulse height distributions in a bounded water medium

1. THE EXPERIMENTAL SET-UP

In radiological applications of ionizing radiation frequently geometries are found in which a radioactive source is immersed within a bounded medium, such as the human body. Examples of such geometries are those found in the therapeutic uses of radio-applicators and in the therapeutic uses of radioactive nuclides which are taken up selectively in one or more organs (*e.g.* ^{131}I in the thyroid). In these cases it would be interesting, from the dosimetric point of view, to measure photon energy distributions in different parts of the body. However, the performance of such measurements in living objects being extremely difficult, such measurements have to be carried out in phantoms. If the measurements were carried out in simple geometries, such as a point source in an infinite medium or in a cylindrical bounded medium, the problem could be investigated more basically. Comparison with calculated data then becomes possible. Moreover, such simple geometries are found in reactor shielding problems. Therefore it is meaningful to start with measurements in such simple geometries. Such measurements are described in this chapter.

Photon energy distributions arising from scattering of ^{137}Cs gamma rays were measured with a point isotropic source geometry in a cylindrical water medium. ^{137}Cs, emitting monoenergetic gamma rays of 0.66 MeV, was chosen as the nuclide for the source instead of the nuclide ^{60}Co, which is used more in the radiological field. The radiation of ^{60}Co, however, comprises gamma radiation of two different energies which complicate the correction of the measured pulse height distributions to a great extent.

Referring to fig. II–1, the 'phantom' used in the present experiments was a polythene cylinder with a diameter of 0.5 m and an altitude of 0.8 m (respectively equal to about 4 and about 7 mean free path lengths for 0.66 MeV gamma rays in water). The cylinder was completely filled with water. Polythene was chosen as the containing material in order to diminish additional boundary effects, the average atomic number of polythene being in the same order of magnitude as that of water. In this cylinder a ^{137}Cs 'point source' (see section II.4) was located on the central axis at a

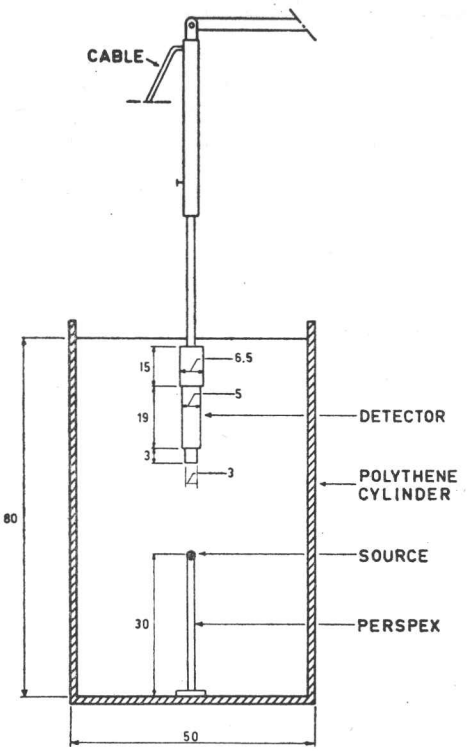

Fig. II–1. Schematic view of the measuring set-up with point isotropic source geometry. Measures in cm.

distance of about 0.3 m from the bottom. A scintillation detector can be moved up and down along the central axis. The scintillation detector is part of a single channel scintillation spectrometer, which is described in section II.3.

With the measuring set-up, described above, pulse height spectra at different source–detector distances were measured in order to investigate the photon energy distributions at these source–detector distances. The distances are conveniently expressed in the number of mean free path lengths of the 0.66 MeV gamma radiation of the source in water ($=\mu_0 r$, in which μ_0 is the linear attenuation coefficient in cm^{-1} for 0.66 MeV photons in water and r is the measuring distance, as defined in section II.4, in cm). Three pulse height spectra were measured, respectively at distances of 1, 2, and 3 mean free path lengths from the source.

Although calculations according to the moment method (see chapter I) strictly spoken are only valid for infinite homogeneous media, the experimental results were compared with these calculations. That such a comparison can reasonably be made, is shown by 'Monte Carlo' calculations of Berger and Spencer (1959).

In the sections II.2, II.3, and II.4 the experimental conditions are described in more detail, while in section II.5 the resulting measured pulse height spectra are given.

2. THE SCINTILLATION CRYSTAL

The absorption of the photon energy depends upon the nature of the interactions in the scintillating material. If the scintillating material has the same or nearly the same atomic properties as has the medium to be measured, the observed pulse height distribution is approximately equal to the electron energy distribution in the medium. For this reason an organic crystal such as anthracene could be used in examining water as a scattered medium. This has been done by Bruce *et al* (1955) and Hayward (1952). A disadvantage of anthracene, however, as Taylor *et al* (1951) have shown, is its non linear response to electrons of energy less than 0.12 MeV. Most of the other organic scintillating materials now available have a relatively low light yield (Ram, 1956) and thus a relatively bad resolving power, which is unfavourable in respect of spectrometric uses. In inorganic crystals, consisting of high Z materials, the atomic photoelectric effect is predominant in the energy range considered here. Nevertheless corrections for escape effects are still needed. Among these materials sodium iodide activated with thallium still is the most suitable for spectrometric purposes (Hofstadter, 1948). It has a linear response to electrons of energy higher than 1 keV (Taylor, 1951), it is easy to crystallize and its transparency to light is excellent.

Though in such a NaI/Tl crystal photoelectric absorption is predominant, part of the incident photon energy still escapes from the crystal. The amount of the escaped photon energy depends on the size of the crystal. The use of a large crystal will generally result in an increased, so called, photopeak efficiency (see chapter III). Maeder *et al* (1954) as well as Lazar *et al* (1956) have shown, however, that using a crystal that has a diameter and thickness of 3 inches, the photopeak efficiency for the gamma radiation of ^{137}Cs is not more than 40%; thus even with crystals of this size a correc-

tion for the escape of scattered photons is needed. Moreover, the use of large detectors in spectrometry of energy distributions in scattering media entails an increased light absorption which affects the resolution unfavourably. In addition errors due to the displacement of the medium by the detector may be enlarged. The use of very small scintillation crystals also may be disadvantageous, for if the radius of the crystal is much smaller than that of the photomultiplier window, the backscatter against the latter may increase inconveniently.

Another point of consideration in respect of the dimensions of the crystal may lie in the requirements of isotropicity. An ideal isotropic crystal has the form of a sphere. However, even if spherical NaI-crystals were available, mounting on a photomultiplier tube would require an (accurately finished) light guide, as a result of which the pulse height, and consequently the resolving power of the detector, would be reduced. The use of a cylindrical crystal, the diameter of which being equal to its thickness, may approximate an isotropic arrangement (see section V.2).

As a consequence of these considerations a NaI/Tl crystal of $^3/_4$ inch diameter and $^3/_4$ inch thickness, adapted to a photomultiplier with a 1 inch diameter window was used in the experiments described.

3. THE SPECTROMETER

The scintillation spectrometer used in the experiments comprises a scintillation detector, an amplifying and pulse shaping stage, a pulse height analyzing stage and a scaling and recording stage.

The detector assembly, a schematic cross sectional view of which is given in fig. II–2, is constructed to be water and light tight. It is composed of three major parts, which are the scintillation crystal, the photomultiplier and the cathode follower, the latter being a 'White' circuit.

The scintillation crystal is a NaI/Tl crystal, type Harshaw 3D3, with a diameter, equal to its thickness, of $^3/_4$ inch. The crystal was cased in a 0,032 inch thick, type 1100 aluminium can, with a reflection layer of packed Al_2O_3, approximately $^1/_{16}$ inch thick. The can was covered by a $^1/_8$ inch quartz window.

As shown in fig. II–2 the crystal was mounted directly on the photomultiplier window, the optical coupling being secured with the aid of 'Dow Corning' stopcock grease, which is a silicone lubricant. The ad-

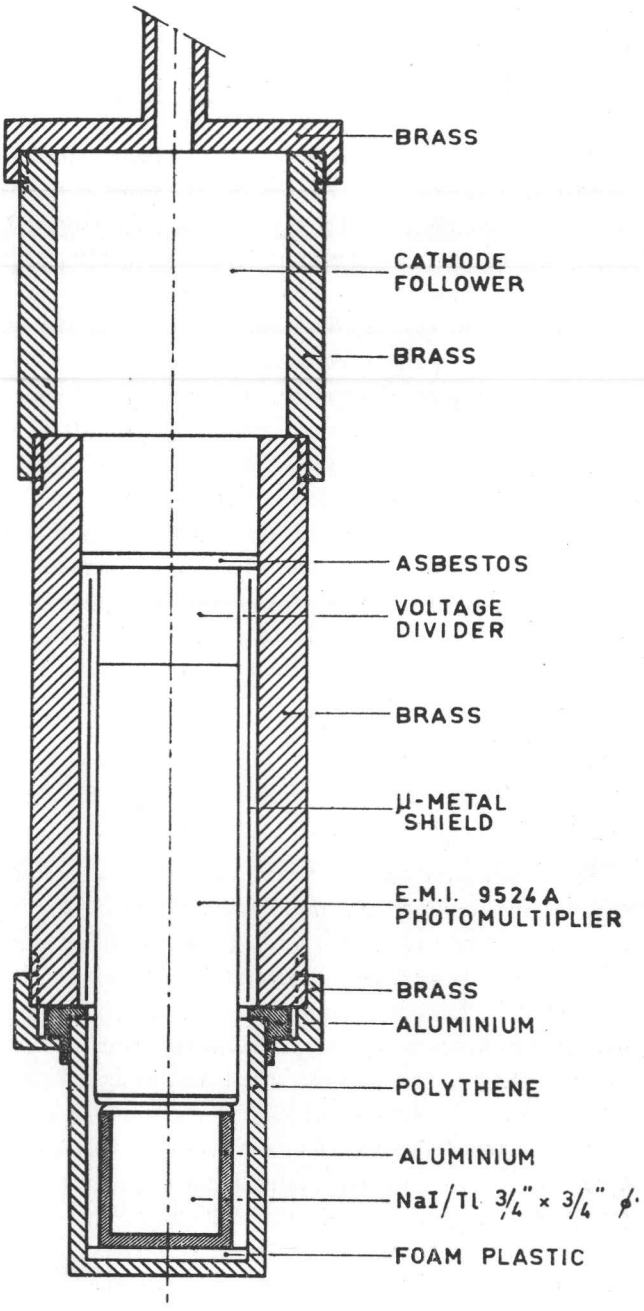

Fig. II–2. Schematic cross sectional view of the detector assembly.

vantage of using this grease instead of the more usual silicone oils is that it can be applied in much thinner layers and enables an easier mounting and demounting of the assembly. In practice this results in a better chance of good resolution powers.

The photomultiplier is an 11 stage, type E.M.I. 9524A photomultiplier with a box-and-grid multiplier system, a SbCs photocathode, and a 1 inch diameter soda glass window. The photomultiplier was specified as selected on the homogeneity of its photocathode. The voltage on the dynodes of the photomultiplier was obtained from a voltage divider (see fig. II–3), the elements of which being chosen such, that the electron current through the photomultiplier tube is small compared to the current in the voltage divider, the maximum ratio of these currents being about 10^{-3}. This arrangement, in addition to the parallel condensors over the last three dynodes, dininishes the influence on the linearity of the voltage drop caused by the pulses on the dynodes. The multiplier system was protected against external magnetic fields by a μ-metal screen.

The output pulses from the anode of the photomultiplier were fed to a 'White' cathode follower circuit (see fig. II–3). This circuit ensures a very high linearity, resulting from its symmetrical circuitry design, and a high stability against changes of the voltage supply. The output impedance Z_0 of this circuit, given by

$$Z_0 = \frac{1}{\mu S}$$

in which μ is the amplification factor and S is the mutual conductance, is extremely low; for the used double triode type E88CC, Z_0 amounts to about 2.5 Ω.

Fig. II–3 is a schematic diagram of the electronic part of the set-up. A coaxial cable with a length of about 5 m served as a connection means between the cathode follower (within the detector assembly) and a linear amplifier, in which the input pulses, after being clipped off by a reflection cable, were amplified. The rise time of the amplifier output pulses was about 0.5 μsec and the pulse duration was about 5 μsec. These pulses were fed to a single channel pulse height analyzer, the output of which being fed, either to a ratemeter which was connected with a recorder, or to a scaler. The channel width of the pulse height analyzer was, in conjunction with adjustment of the triggering level of the upper discriminator, adjustable by means of the variable gain of the back biased input amplifier.

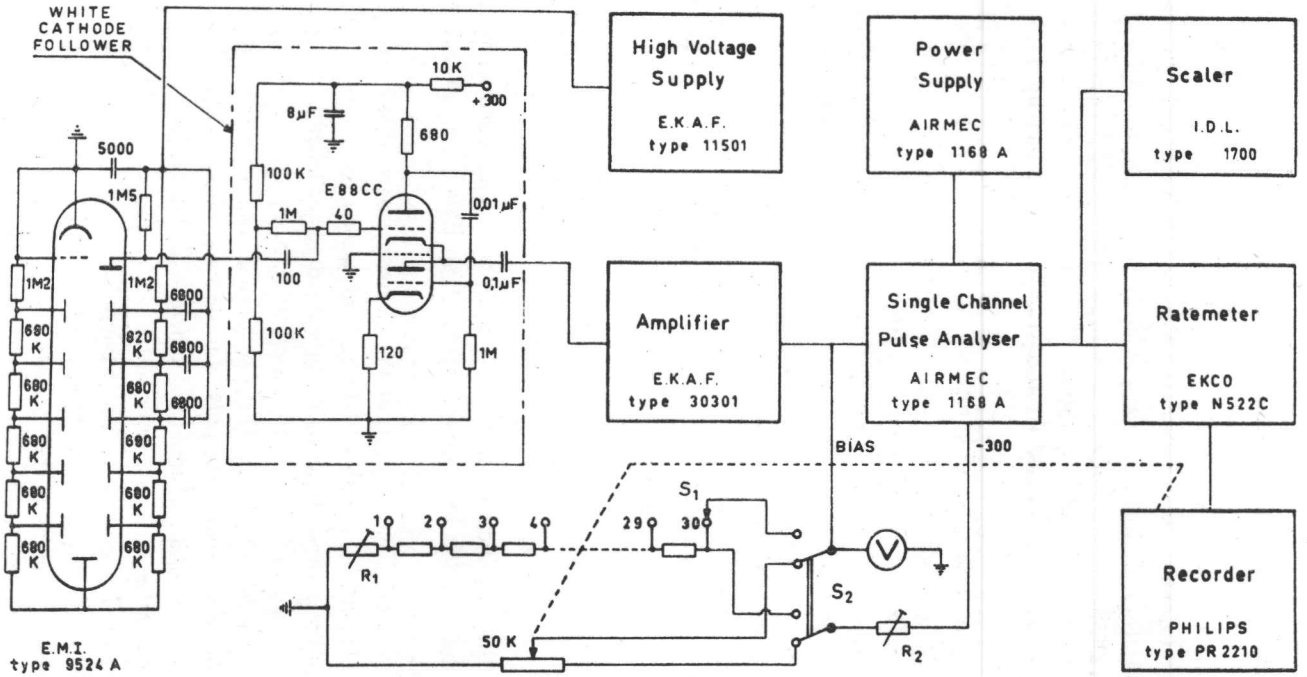

Fig. II–3. Schematic diagram of the electronic set-up.

The scintillation spectrometer can be operated either manually or automatically, in the latter case by means of a motor driven potentiometer. With automatic operation the output of the pulse height analyzer was connected to a ratemeter, which in turn was connected to a recorder. Automatic operation was applied when a high accuracy of the count rate measurements was not necessary. The statistical error in automatic operation never exceeded 5%.

The measurements described in this chapter were carried out with the spectrometer in manual operation. To this purpose the pulse height analyzer was connected to a scaler and the motor driven potentiometer was replaced by a channel number selecting potentiometer, which is adjustable in such a way that a preselected energy range can be scanned in 30 intervals, which are equal to each other within 1%. The adjustment by means of the variable resistances R_1 and R_2 (see fig. II–3) for an energy range between 0.08 MeV and 0.66 MeV was carried out as follows.

The channel number selecting potentiometer was set on channel number 30. Then a ^{137}Cs source was placed near the detector, and R_2 was adjusted such, that the ratemeter read a maximum count rate. This count rate corresponds to that of the centre of the ^{137}Cs photopeak at 0.66 MeV energy. The bias voltage was then measured with the aid of a high input

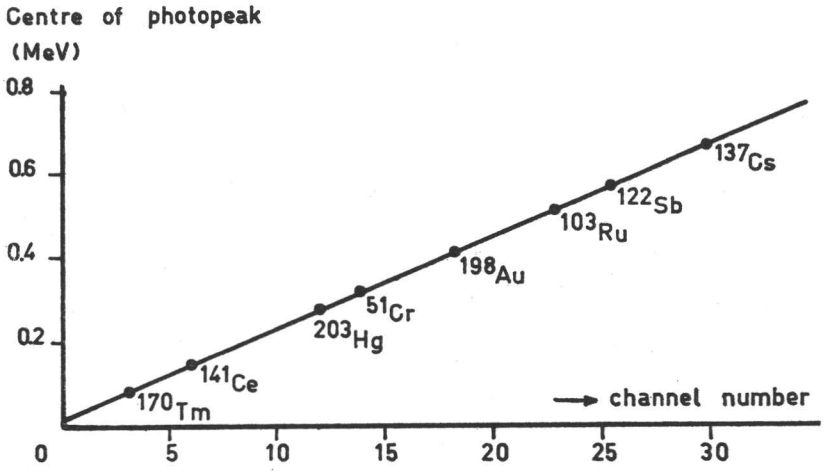

Fig. II–4. Callibration curve of the spectrometer in manual operation.

impedance voltmeter V. From this measured voltage the voltage corresponding to the lower energy range boundary, *i.e.* 0.08 MeV, was calculated. Then the potentiometer was set on channel number 1 and R_1 was adjusted to this calculated voltage. Since the setting of both variable resistances influences the overall bias voltage, the adjustments were repeated until both settings were correct. The adjustments were checked several times during the pulse height measurements. The drift in the electronic apparatus was found to be less than 1% in 8 hours. A calibration curve of the spectrometer, adjusted as described, is given in fig. II–4.

4. THE EXPERIMENTAL POINT SOURCES

In the present experiments spherical ^{137}Cs sources were used. These were prepared by filling glass bulbs, having a diameter of 1 cm, with a solution of $^{137}CsCl$. Such spherical sources may be considered as point sources at the measuring distances of 1, 2, and 3 mean free path lengths as may be apparent from fig. II–5, in which the ratio of the calculated radiation of a point source to the calculated radiation of a

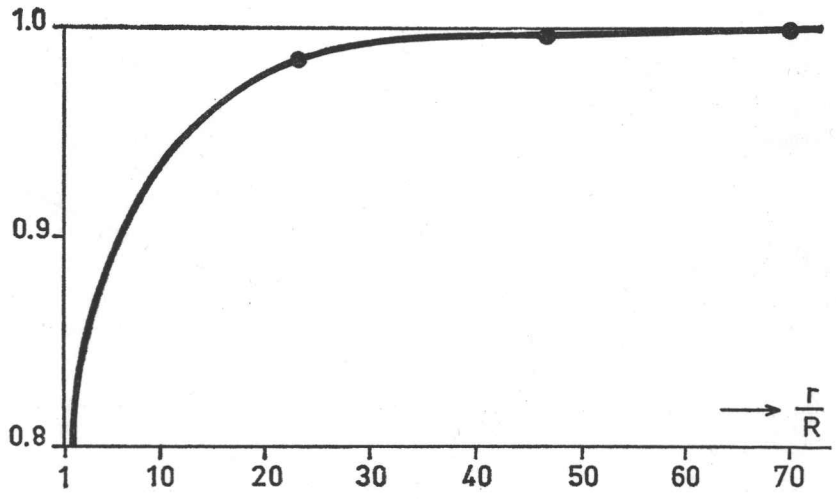

Fig. II–5. Ratio between the calculated radiation of a point source and the calculated radiation of a spherical source with radius R as a function of the relative measuring distance r/R. The dots indicate the actual measuring distances.

spherical source with a radius R is given as a function of the relative measuring distance r/R. The radiation of a spherical source at a distance r can be calculated according to a formula given by Mayneord (1950). The measuring distance was considered to be the distance between the centre of the source and the centre of the scintillation crystal.

To normalize the measured pulse height distributions to a source emitting one photon per second, the source strengths must be known. These source strengths were measured with an ionization chamber by comparing the spherical sources with an identical spherical source containing a standard solution of ^{137}CsCl. The precision of this standard solution, which was obtained from the Amersham Radiochemical Centre, was $\pm$ 2%. The measuring accuracy was about 3%. In the present experiments two sources were used, the strengths of which being respectively 116 $\pm$ 5 μC and 530 $\pm$ 20 μC. The first source was used in measuring the pulse height spectra at the measuring distances of 1 and 2 mean free path lengths, and the second source in measuring the pulse height spectrum at the measuring distance of 3 mean free path lengths.

5. THE DISPLACEMENT OF THE MEDIUM BY THE DETECTOR

The displacement of the medium by the detector during the measurements may cause errors in the results. The scintillation crystal can be considered as the measuring spot itself: the energy distributions of the photons that are incident on the volume that is occupied by the crystal were determined. So the errors arise because of a change in the scattering pattern by the so called 'detector-stem'. This may be the case especially in the set-up of the measurements at penetration distances of 1 and 2 mean free path lengths. With measurements at a penetration distance of 3 mean free path lengths only a small part of the detector was submerged in the medium. In the latter case the neighbourhood of the interface between water and air may be of influence.

To investigate the importance of this type of error some preliminary experiments were carried out. In the first experiment, illustrated in fig. II–6, the stem error for a penetration distance of 1 mean free path length was measured. This was done by measuring a pulse height spectrum in the medium with the source in a horizontal plane through the centre of the detecting crystal, at a distance of 11.7 cm from centre to centre ($\mu_0 r = 1$), and repeating this measurement with a 'dummy stem' coupled

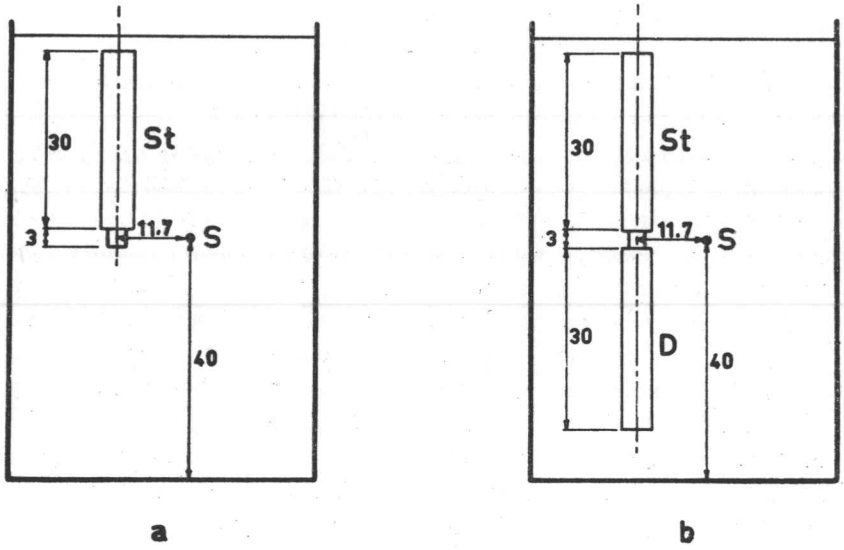

Fig. II–6. Measuring set-up for estimating the stem error at 1 mean free path length. St is the detector stem, S is the source, and D is the dummy stem. Measures in cm.

to the detector. This 'dummy stem' comprises a photomultiplier identical to the one used in the detector, cased in a brass housing with dimensions equal to those of the housing of the detector. The pulse height spectra were measured with the spectrometer in automatic operation (see section II.3).

The first pulse height spectrum can be represented by the set of numbers $y_1 - s_1'$, in which y_1 is the spectrum that would be measured if the influence of the stem were negligible. The second pulse height spectrum can be given by $y_1 - 2s_1'$ (neglecting the mutual influence of the detector-stem and the dummy). Subtracting the first spectrum from the other yields s_1' and the true spectrum y_1. The stem error s_1 for the measurement with the geometry described in section II.1 at a penetration distance of 1 mean free path length was obtained by subtracting the spectrum z_1, measured with such a geometry, from the true spectrum y_1. The resulting stem error s_1 was found to be unmeasurably small in all the channels of the spectrum z_1, except in the two lowest energy intervals, in which s_1 was less than 5% and 7%.

In the second experiment, illustrated in fig. II–7, the detector was located at a distance of 2 mean free path lengths from the source in a

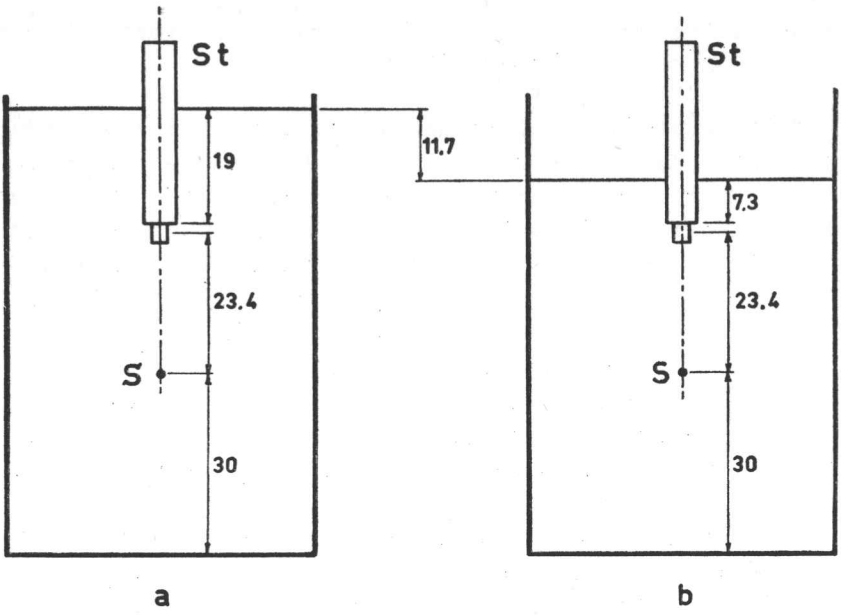

Fig. II–7. Measuring set-up for estimating the stem error at 2 and 3 mean free path lengths. St is the detector stem, and S is the source. Measures in cm.

geometry as described in section II.1. The cylinder was completely filled with water, a large part of the detector being submerged in the water. With such a geometry a pulse height spectrum was measured. Then the water level was lowered over a distance of 11.7 cm (= 1 mean free path length), as a result of which only about 25% of the detector was submerged. Also with this geometry a pulse height spectrum was measured. These two pulse height spectra do not show any difference. Considering this result in combination with the result of the first experiment, it may be assumed that

a. in the proper measurements no stem correction will be needed and
b. there is no important influence of the near interface between water and air on the result of the pulse height spectrum measurement at a penetration distance of 3 mean free path lengths. This may be considered as an experimental confirmation of the calculations of Berger and Spencer (1959) on bounded scattering media (see section I.4).

6. THE MEASURED PULSE HEIGHT SPECTRA

With the experimental set-up described in section II.1 pulse height spectra at penetration distances of 1, 2, and 3 mean free path lengths (the distances between the centre of the crystal and the centre of the source being respectively 11.7 cm, 23.4 cm, and 35.1 cm, and μ_0 in water for 0.66 MeV photons being 0.0859) were measured. The spectrometer was operated manually and was adjusted as is described in section II.3, the channel width being equivalent to 0.02 MeV. In each of the 30 channels the count rate was determined within a statistical accuracy of less than 0.3%, the counting time required being on the average 1000 seconds. The measured count rates were normalized to those resulting from a source emitting one photon per second. These normalized pulse height spectra are given in fig. II–8.

The relation between the measured pulse height spectra and the incident photon energy distributions can be represented by a response equation of the detector. This equation and its solution are discussed in the chapters III, IV, and V. The resulting photon energy distributions are given in chapter VI.

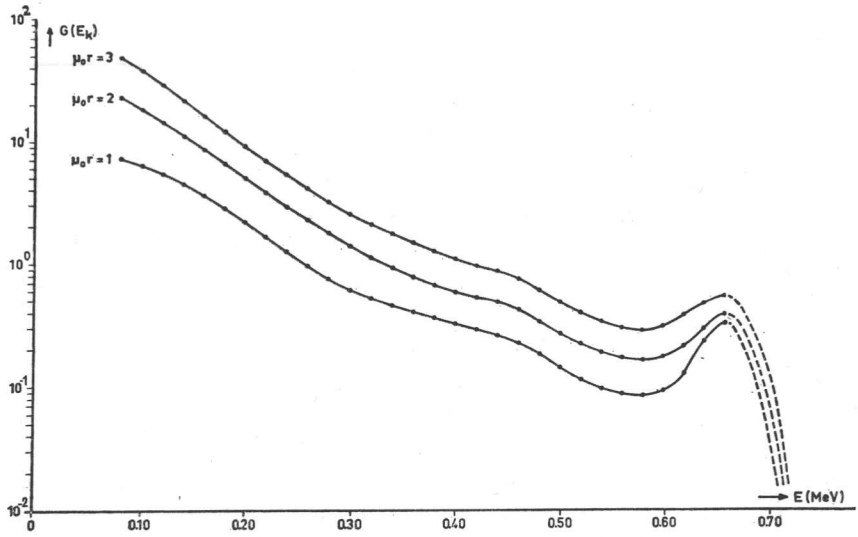

Fig. II–8. Pulse height spectra $G(E_k)$ of scattered 0.66 MeV photons in a cylindrical water medium with point isotropic source geometry at three penetration distances in the medium.

CHAPTER III

The interpretation of the measured pulse height spectra

1. INTRODUCTION

The relation between the pulse height distributions, measured as described in the previous chapter, and the incident photon energy distributions is not a simple proportionality. In the first place not all of the incident photon energy is absorbed in the scintillating material, the rate of absorption being energy dependent. Furthermore the spread in pulse height is also energy dependent. Therefore this relation itself is determined by the incident photon energy. Also the shape, size and nature of the scintillating material influence this relation.

If monoenergetic photons with energy $E < 1$ MeV are incident on a sodium iodide crystal, part of these are subject to photoelectric interactions and others to compton interactions in the material. Since an incident photon energy $E < 1$ MeV is lower than the equivalent energy of two electrons, pair production does not occur. As a result of photoelectric interactions an electron having a kinetic energy of $E - \Phi$, in which Φ is the binding energy of the electron, is ejected and the atom involved is left in an excited state. If one of the outer electrons 'falls into the hole' fluorescent radiation is emitted. If the fluorescent radiation is absorbed in the material its energy also is converted to electronic motion, and the total electron kinetic energy is E. Compton interactions produce free electrons in a continuous range of energy as a result of the escape of scattered photons. This energy range has a maximum value which is determined by the laws of conservation of energy and momentum.

The free electrons in the crystal, having an energy distribution resulting from these processes fall into defined excited levels and as a result of recombination processes (in which the activator plays an important role) luminescent radiation is emitted. Luminescent quanta falling upon the photocathode of the photomultiplier produce photoelectrons and the generated photoelectron current is amplified by secondary emission. As a result output pulses can be taken from the anode, the amplitudes of which are, disregarding the spread in the pulse height, proportional to that part of the incident photon energy that is absorbed in the crystal. It can

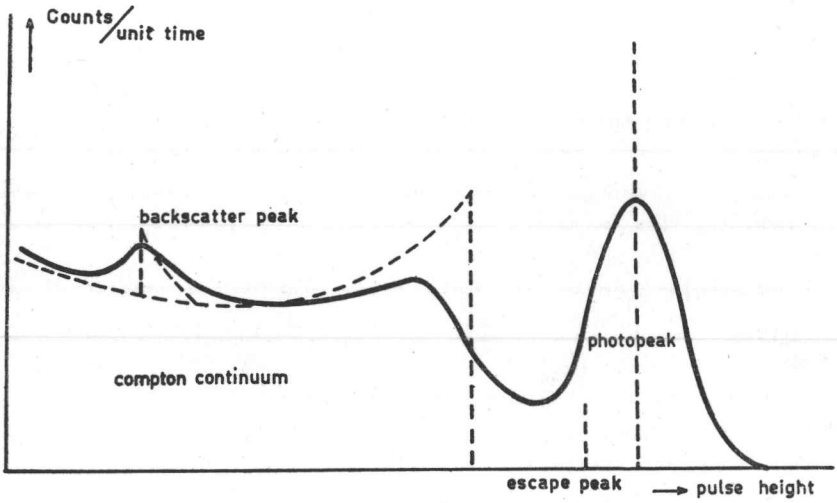

Fig. III–1. Schematic pulse height spectrum. Dashed line: electron kinetic energy distribution within the scintillation crystal.

be proven experimentally that the statistical spread in the pulse height is approximately normal. The statistical spread limits the resolving power of the detector, a measure of which being given by the relative half width of the photopeak, *i.e.* the ratio between the width of the photopeak at half maximum and the position of the centre of the peak.

A schematic monoenergetic pulse height spectrum is shown in fig. III–1. The dashed line in the figure shows the energy distribution of the recoil electrons in the crystal. Typical characteristics of the spectrum are the *photopeak*, the *escape peak* and the *compton continuum*. The photopeak is composed of pulses which are generated by electrons with total energy E. The escape-peak, which can only be resolved from the photopeak at photon energies less than about 0.2 MeV, is composed of pulses which result from electrons with energy $E - \Phi$. The compton continuum comprises those pulses, which are generated by compton recoil electrons after the escape of the scattered photons. A spurious peak, the backscatter peak, appears in the low energy range of the spectrum, due to backscattering of photons, mostly at the glass window of the photomultiplier.

If secondary processes would not occur in the crystal, the ratio between the area of the photopeak and the area of the spectrum, the so called *photopeak efficiency*, would be equal to the relative photoelectric proba-

bility (see section III.3). The occurrence of secondary processes generally increases the photopeak efficiency, because when *e.g.* a compton process is followed by photoelectric absorption of the scattered photon the initial photon is counted in the photopeak.

2. THE RESPONSE EQUATION

If a continuous energy spectrum of photons $S(E')$ is incident upon the detector of a scintillation spectrometer, the observed pulse height distribution $G(E)$ is related to it according to the equation

$$G(E) = \int_0^{E_0'} K(E,E')S(E')dE' \qquad \text{(III–1)}$$

in which E_0' is the maximal energy present in the incident spectral distribution.

Equation III–1 is an integral equation for $S(E')$ of the first kind, in which the kernel $K(E,E')$ is a response function such that

$$K(E,E')dE$$

is the probability that an incident photon with energy E' will produce an output pulse between E and $E + dE$.

The mathematical problem of finding useful conditions which are necessary and sufficient for the existence of a unique solution of equations of the type of equation III–1 still is unsolved. If the kernel $K(E,E')$ were symmetric, the conditions which are sufficient could be expressed in terms of the eigenvalues and eigenfunctions of the kernel. In that case one could prove that if the function $G(E)$ could be expanded as

$$G(E) = \sum_{n=1}^{\infty} a_n \varphi_n \qquad \text{(III–2)}$$

in which φ_n are the eigenfunctions of the kernel K, the solution of equation III–1 would be given by

$$S(E') = \sum_{n=1}^{\infty} a_n \lambda_n \varphi_n \qquad \text{(III–3)}$$

in which λ_n are the eigenvalues of the kernel provided that the series III–3 converges uniformly (Whittaker and Watson, 1958). If the kernel is non symmetric, necessary and sufficient conditions can in general be expressed, according to the law of Picard, in terms of Schmidt functions (Courant and Hilbert 1931), the existence of a solution of equation III–1, of course, greatly depending on the behaviour of the kernel.

The main difficulty that is encountered here is the fact that the function $G(E)$ is not analytically defined but is given merely as a set of numbers

$$G(E_k) = \frac{1}{\Delta E} \int_{E_k - \frac{1}{2}\Delta E}^{E_k + \frac{1}{2}\Delta E} G(E)dE \qquad \text{(III–4)}$$

$$(k = 1, 2, 3, \ldots n)$$

in which n is the number of channels and ΔE is the channelwidth.

Suppose now that $G(E)$ can be fitted with a partial sum $G(E_k)$ of orthonormal functions φ_1

$$G(E_k) = \sum_{i=1}^{k} c_1 \varphi_1 \qquad \text{(III–5)}$$

in which

$$c_1 = \int G(E)\varphi_1 dE \qquad \text{(III–6)}$$

If the inverse transform of φ_1, denoted bij Φ_1, is known, then the transform of

$$S(E_k) = \sum_{i=1}^{k} c_1 \Phi_1 \qquad \text{(III–7)}$$

is $G(E_k)$. If k is sufficiently large, the $S(E_k)$ of III–7 will satisfy the integral equation III–1 arbiratrily closely in the sense of a least square approximation. If, however, the sequence $S(E_k)$ diverges, the solution cannot be considered as a good approximation to the true solution of equation III–1, as clearly is demonstrated in an example by Dixon and Aitken (1958). The establishment of the convergence or divergence of the sequence $S(E_k)$ is, however, very difficult, because the coefficients c_1 are given only numerically.

The solution method used by Theus *et al* (1955) consists of replacing the integral equation III–1 by a set of linear equations

$$G(E_k) = \sum_{j=1}^{n} K(E_k,E_j)S(E_j)\Delta E \qquad \text{(III–8)}$$

$$(\Delta E = E_j - E_{j-1})$$

of which equation III–1 is the limit for $n \to \infty$.

If the determinant of the matrix $\mathbf{K}_{k,j}$ is non vanishing in the limit case, there exists a unique inverse matrix $\mathbf{K}^{-1}_{k,j}$ such that

$$S(E_k) = \sum_{j=1}^{k} K^{-1}(E_k,E_j)G(E_j)\Delta E \qquad \text{(III–9)}$$

which is an approximation to

$$S(E) = \int_0^{\infty} K^{-1}(E,E')G(E')dE' \qquad \text{(III–10)}$$

in which $K^{-1}(E,E')$ is the inverse kernel of the integral equation III–1.

While numerical methods of this kind can be used for the solution of Volterra integral equations (in which $E \leqslant E'$) and Fredholm integral equations of the *second kind* (Whittaker and Watson, 1958), the general applicability to integral equations of the *first kind* is not mathematically proven, the existence of an inverse kernel as in equation III–10 greatly depending on the character of the kernel $K(E,E')$. Knowledge of the behaviour of $K(E,E')$ therefore is necessary. In the next section this kernel is examined in more detail.

3. FACTORS DETERMINING THE KERNEL

The kernel $K(E,E')$ of the integral equation III–1 is generally determined by three functions, *i.e.* a function $\varepsilon(E')$ representing the probability of interaction of the incident photons, a function $k(x,E')$ representing the probability that after interaction of a photon with energy E' an electronic kinetic energy between x and $x + dx$ is produced, and a function $N(E,x)$ representing the statistical spreading. This kernel is given by

$$K(E,E') = \varepsilon(E') \int_0^{E'} N(E,x)k(x,E')dx \qquad \text{(III–11)}$$

The function $\varepsilon(E')$, defined as the *total efficiency* (to be distinguished from the photopeak efficiency), depends upon the geometry of the experimental set-up. When a parallel beam is incident upon a flat side of the crystal, the total efficiency is given by

$$\varepsilon(E') = 1 - e^{-\mu_t d} \qquad \text{(III–12)}$$

in which μ_t is the total attenuation coefficient of the scintillating material and d is the thickness of the crystal. If the incident beam is departing from a point isotropic source which 'sees' the crystal under a certain solid angle, the total efficiency can be calculated according to Wapstra (1953). When photons are incident from alle directions, exact calculation of the total efficiency is very tedious. In that case the total efficiency may be approximated by considering the crystal to be purely isotropic, *i.e.* the total efficiency to be independent from the direction of incidence of the photons (see section V.2). In all cases the function $\varepsilon(E')$ may be considered as continuous and limited between 0 and 1, for energies larger than the K-energy of iodine (0.033 MeV).

The function $k(x,E')dx$, which is determined by the processes of photon energy absorption and by the rate at which these processes occur, can be represented by

$$k(x,E')dx = p\{(1-q)\delta(E'-x) + q\delta(E'-\Phi-x)\}dx + (1-p)X(x,E')dx \qquad \text{(III–13)}$$

in which p is the ratio of the joint areas of the photopeak and the X-ray escape peak to the area of the spectrum, q is the ratio of the area of the X-ray escape peak to the area of the photopeak, $\delta(\ )dx$ are Dirac delta functions, and $X(x,E')dx$ is a function representing the probability of an electronic kinetic energy between x and $x + dx$ after compton interaction and escape of the scattered photons.

If any secondary absorption in the crystal is neglected, the factor p is given by

$$p = \frac{\tau}{\tau + \sigma} \qquad \text{(III–14)}$$

in which τ is the photoelectric cross section and σ is the compton cross section. In that case the function $X(x,E')dx$ can be derived directly from the Klein Nishina differential cross section for compton scattering (Heitler, 1954). The factor q can be calculated for relatively simple geometries (Axel, 1953). If secondary interactions do occur the factor p can be determined experimentally. If secondary interactions mainly consist of photoelectric absorption after compton scattering, the function $X(x,E')dx$ still can be derived from the Klein Nishina formula. If also the escape of photons, which are scattered more than once, is to be considered, the picture becomes more complicated. While p can still be determined experimentally, the Klein Nishina formula for $X(x,E')dx$ no longer holds, for the energy distribution of compton recoil electrons is changed more or less considerably. In chapter V a method is set forth, by which the function $X(x,E')dx$ can be evaluated experimentally.

The function $N(E,x)$ can be considered as a Gaussian distribution function

$$N(E,x) = \frac{1}{C} \exp\left\{ -\frac{1}{2v_Q}\left(\frac{E-x}{x}\right)^2 \right\} \qquad \text{(III–15)}$$

in which C is a normalisation factor and v_Q is the relative variance in pulse height. This relative variance is often assumed to be inversely proportional to the absorbed energy x (Dixon 1958). This may be a good approximation for electrons generated by incident photons up to 0.2 MeV. However, at higher energies this approximation no longer confirms the observations (Kelley *et al*, 1956). Observations of Bisi and Zappa (1958) indicate a relation

$$v_Q = \alpha + \beta/x \qquad \text{(III–16)}$$

in which α and β are constants which are related to statistical effects in the crystal itself as well as in the photomultiplier. The relation III–16 seems to be confirmed by our observations (see section IV.3) as well as those of Wapstra (1953). A more detailed discussion about the function $N(E,x)$ is given in chapter IV.

The integration of III–11 being carried out, the kernel $K(E,E')$ becomes a continuous function of the variables E and E'. If E' is taken as a constant, the function $K(E)_{E'}$ has a form similar to that of a monoenergetic pulse height spectrum as shown in fig. III–1 (drawn line).

Corrections for backscatter against parts of the detector may be incorporated in the kernel K of the integral equation III–1. As will be seen later (section V.6) this correction can be obtained from experimental data and added to the function $k(x,E')$ as defined by III–13. Calculations as have been carried out by Lidén and Starfelt (1954) are rather tedious and inadequate to geometries as considered here.

4. DIFFICULTIES IN SOLVING THE RESPONSE EQUATION

As may be apparent from the previous section, the kernel $K(E,E')$ of equation III–1 is a continuous, non symmetric function of the variables E and E'. Therefore the solution of III–1 cannot be obtained in the form of an expansion in eigenfunctions of the kernel, according to equation III–3.

As has been mentioned, one of the functions determining the kernel $K(E,E')$ is the exponential function $N(E,x)$, given by equation III–13. This function causes great difficulties in solving the integral equation III–1. The factor $k(x,E')dx$, as defined by equation III–1, does not give rise to difficulties, as it can be considered as a kernel of a Volterra integral equation in which $x \leqslant E'$. A matrix constructed from this function is a triangular matrix, none of the diagonal elements of which in general tends to become zero. Hence this kernel may be inverted without any difficulty.

So if the measured pulse height distributions are first corrected for the limited resolution, the correction for escape effects in the crystal may then be carried out in arbitrarily close approximation. To do such a separated correction, we define a function $g(x)$ which describes the energy distribution of the liberated electrons in the crystal. This energy distribution is related to the incident spectrum according to

$$g(x) = \int_{x}^{E_0'} \varepsilon(E')k(x,E')S(E')dE' \qquad \text{(III–17)}$$

which is a Volterra integral equation and can be approximated by

$$g(x_1) = \sum_{j=i}^{n} \varepsilon(E_j)k(x_1,E_j)S(E_j)\Delta E \qquad \text{(III–18)}$$

where $\Delta E = E_j - E_{j-1}$ and $x_i = E_j$ if $i = j$, the approximation being closer when n increases.

The relation between the electron energy distribution $g(x)$ and the observed pulse height distribution $G(E)$ is given by

$$G(E) = \int_0^{E_0'} N(E,x)g(x)dx \qquad \text{(III–19)}$$

For some classes of functions $G(E)$ analytical solutions of equation III–19 may be obtained. Making use of these partial solutions a general solution in terms of Hermite polynomials can be obtained, as Dixon and Aitken (1958) have shown. However, as the function $G(E)$ is only given numerically, the evaluation of the higher derivatives, required for the use of this analytical solution, leads to large uncertainties. Fitting $G(E_k)$ by a series of orthonormal functions (for example by a Fourier series), the transform of which is known, the transformed series clearly tends to diverge, due to the exponential factor in the transform. Therefore solutions of the form of III–7 give rise even to still larger uncertainties.

In practice there seems to be no method for a complete and unique solution of equation III–19, unless the existence of an inverse kernel is demonstrated, which is unlikely. Additionally the lack of analytic definition in $G(E)$ always gives rise to enlarged uncertainties. While an approximation to the solution of an integral equation which only describes escape effects (equation III–17) can be arbitrarily close, the resolution correction must be restricted to sharpening the peaks and the valleys already present in the observed pulse height spectrum $G(E)$ and is unable to solve the fine structure in the incident photon energy spectrum $S(E')$. This may be clear from the fact that spreading effects in the crystal and in the photomultiplier destroy information, collected in the crystal by the ionization processes.

However, sharpening the peaks and the valleys still may be very useful to yield data about incident continuous energy spectra. If the resolution correction method is subject to the mentioned restriction, an approximate solution by numerical methods may be obtained, provided that the determinant of the involved matrix is sufficiently large. In chapter IV such a correction method is carried out, while in chapter V the correction for the escape effects is discussed. Both corrections are applied to the pulse height distribution measurements of scattered photons, described in chapter II.

CHAPTER IV

The resolution correction

1. INTRODUCTION

To obtain an approximation of the solution of equation III–19 (see section III.4) one could try to replace this equation by a set of linear equations

$$G(E_k) = \sum_{i=1}^{n} N(E_k,x_i)g(x_i)\Delta x \qquad \text{(IV–1)}$$

in which $\Delta x = x_i - x_{i-1}$ and $E_k = x_i$ for $k = i$.

The solution of such a set of equations can be obtained by matrix inversion or by iterative procedures, provided that the matrix **N** is in a reasonable condition.

As has been mentioned in the previous chapter the resolution correction by these methods can only involve sharpening of the peaks and valleys *already present* in the observed pulse height spectrum. The problem of getting a pulse height spectrum which yields as much information as possible of the incident photon energy distribution is a pure instrumental one, the differentiation in the pulse height spectrum being governed by the relative variance v_Q in the pulse height. This relative variance is an overall variance resulting from several processes such as luminescence in the crystal, transference of light through the crystal and the lightguide, conversion of light into photoelectrons in the photocathode of the photomultiplier, collection of photoelectrons at the first dynode, and secondary emission in the photomultiplier. In the next section these processes are discussed in as much as they influence the final result, while a description of the experimental determination of the relative variance v_Q will follow in section IV.3.

2. THE SPREAD IN PULSE HEIGHT

Fast charged particles, as electrons liberated by ionization processes after incidence of gamma radiation, cause luminescence in scintillating

materials, such as monocrystals of NaI, activated with traces of Tl. About these luminescence processes an extensive literature is now available, a summary of which is given by Parmentier (196). However, a thorough0 treatment of this subject falling out of the scope of this thesis, only the essentials are given shortly and in a superficial way.

The electrons liberated by ionization processes in the crystal cause a sequence of excitations, as a result of which electrons appear in the conduction shells of the atoms in the crystal-lattice. An electron in such a conduction shell can move freely through the crystal, which is also the case for the resulting positive hole in the lattice. When both the electron in a conduction shell and the positive hole in the lattice reach an activator centre (electron trap), recombination may occur as a result of which either fluorescent or phosphorescent radiation is emitted, or the excitation energy is quenched. Quantitative analysis of these processes is very difficult, but as we are only interested in the overall effect, the important quantity here is the fraction of the exciting energy that is converted into luminescent energy. This fraction, the so called conversion or intrensic efficiency η can be regarded as a constant for exciting electrons down to 1 keV in NaI/Tl crystals, as is apparent from the experiments of Taylor *et al* (1951). Then the average number of luminescent quanta $\bar{L}$ that are emitted as a result of a certain kinetic energy x of exciting electrons in the crystal is given by

$$\bar{L} = \frac{\eta x}{h\bar{\nu}} = \bar{e}x \qquad \text{(IV–2)}$$

in which $h\bar{\nu}$ is the averaged luminescent energy. The quantity e can be considered as the number of luminescent quanta emitted per MeV, the mean and the relative variance of e being respectively $\bar{e}$ and v_e. A fraction f of these luminescent quanta will reach the photocathode of the photomultiplier. If one luminescent quantum generates g photoelectrons, a fraction c of which being collected at the first dynode, the number of photoelectrons that start the secondary emission after a scintillation will be

$$q = cgfex = tex \qquad \text{(IV–3)}$$

in which $t = cgf$ is the *transfer efficiency*. The quantities c, g and f are stochastic quantities, each of them fluctuating according to some proba-

bility distribution function. However, they are mutually dependent, the relations between them being a consequence of the varying localisation of the individual scintillations, the varying chromatic distribution of the luminescent quanta, the optical properties of the crystal, the reflection layers and the lightguide, and the inhomogeneities of the photocathode. Therefore it is impossible to treat these factors separately and the transfer efficiency t has to be considered as a whole. The values of t fluctuate about a mean $\bar{t}$, these fluctuations being described by a relative variance v_t.

The secondary emission at the successive dynodes amplifies the electron current in the tube, the amplification factor of each stage also being subject to statistical fluctuations. If the total amplification factor of the photomultiplier is denoted by A, we can say that A fluctuates about a mean $\bar{A}$ with a relative variance v_A. As Bisi and Zappa (1958) have shown, the occurring aftereffects in the photomultiplier after a secondary electron avalanche can be taken into account if the collection time at the anode of the photomultiplier is large enough to add up the primary and afterpulses.

Now the fluctuation of the total number of secondary electrons, arriving at the anode of the photomultiplier

$$Q = Atex$$

given by the relative variance v_Q, can be expressed, using the statistical moment generating functions. According Bisi *et al* (1958) this relative variance is given by

$$v_Q = v_t + (1 + v_t)\left(v_e - \frac{1}{\bar{e}x}\right) + \frac{1+v_A}{\bar{e}\bar{t}x} \qquad \text{(IV–4)}$$

assuming that the probability distribution of Q is normal in a good approximation, which is shown experimentally (see fig. IV–1). Assuming further that the variance in e is according to a Poisson distribution ($v_e = 1/(\bar{e}x)$) equation IV–4 is reduced to

$$v_Q = \alpha + \beta/x \qquad \text{(IV–5)}$$

in which

$$\alpha = v_t \qquad \text{(IV–6)}$$

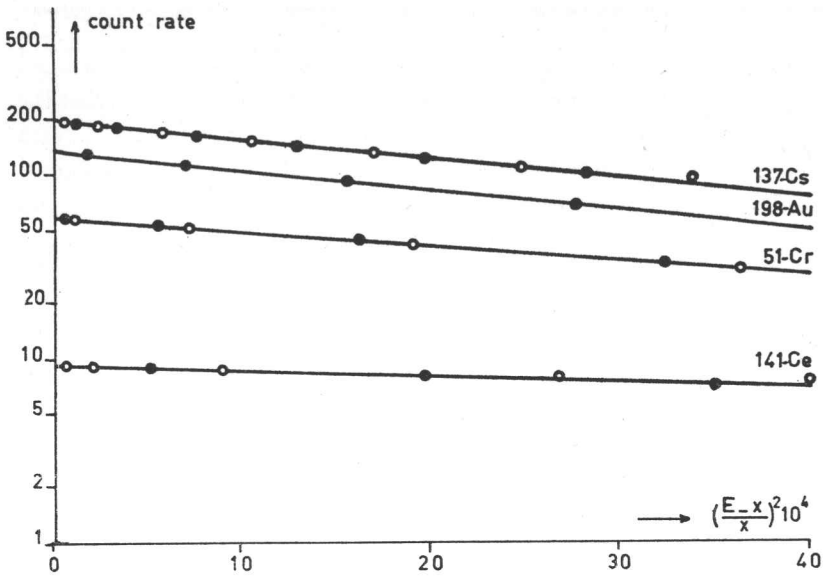

Fig. IV–1. Semi-logarithmic plot of the count rate in the photopeak as a check of the gaussian shape of the peak. Open circles: low energy part of the peak; closed circles: high energy part of the peak.

and

$$\beta = \frac{1 + v_A}{\bar{e}\bar{t}} \qquad \text{(IV–7)}$$

The constants α and β can be considered as instrumental constants of a particular detector. The crystal as well as the optical coupling and the photocathode of the photomultiplier contribute to the value of both constants.

De Waard (1955), following an analogeous reasoning, arrived at a different expression for the relative variance in the number of electrons, arriving at the anode of the photomultiplier. This expression has the form

$$v_Q = a.b.1/x \qquad \text{(IV–8)}$$

In this expression the constant a is equal to the relative variance in the number of electrons that is liberated in the photocathode and the constant b gives the contribution of the photomultiplier, as a consequence of the

incomplete collection of electrons on the dynodes and the statistical spread in the secondary emission. However, also De Waard pointed out that equation IV–8 does not fit in experimental observations and that the relative variance in the pulse height rather has to be expressed in a form as given in equation IV–5. However, in view of the considerations given above, it seems to be wise not to consider the constant α as due only to impurities in the crystal, the optical coupling, and the photocathode of the photomultiplier, but to consider α as well as β as influenced by statistical processes in the scintillation detector as a whole. Anyhow both constants can be seen as instrumental constants of a particular assembly of a scintillation crystal and a photomultiplier.

The relative variance v_Q is equal to the relative variance in the pulse height, provided that extraneous sources of pulse height fluctuation are negligible. This is the case if

a. the supply voltage of the photomultiplier is very constant;
b. the fluctuations in the supply voltage due to the pulse are negligible;
c. the influence of external magnetic fields is reduced to a negligible amount;
d. the drift in the electronic equipment is negligible during a period comparable with the counting time;
e. the channel width of the analyzer is such, that it does not enlarge the line width.

The constants α and β being known, formula III–5 can be used to calculate the matrix **N** for solving the set of equations IV–1.

3. EXPERIMENTAL DETERMINATION OF THE DETECTOR CONSTANTS

The constants α and β were determined by measuring the photopeaks of a number of nuclides (see table I) and determining the relative variance of each photopeak. An experimental check of the gaussian shape of the peaks can be obtained by plotting the logarithm to the base 10 of the counting rate $M(E_k)$ against $(E_k-x)^2/x^2$, in which x is the energy of the incident photons involved. If the line shape is gaussian these plots must yield straight lines. In fig. IV–1 such plots are given. From these plots also the experimental line widths in terms of the relative variance v_Q (assumed to be equal to the relative variance in the pulse height) can be

derived (Villforth *et al*, 1958), for the counting rate of the points in a separated photopeak being given by $M = cN(E,x)$, in which $N(E,x)$ is the normal probability function of III–15 and c is a constant, the slope of these straight lines is

$$\frac{\log e}{2 v_Q}$$

from which v_Q can be determined.

Nuclide	Gamma ray energy (MeV)	$v_Q \cdot 10^4$	w %
$^{60}_{27}$Co	1.33	6.8	6.1
$^{60}_{27}$Co	1.17	10.4	7.6
$^{137}_{55}$Cs	0.66	14.3	8.9
$^{122}_{51}$Sb	0.57	15.5	9.3
$^{103}_{44}$Ru	0.50	17.9	10.0
$^{198}_{79}$Au	0.41	21.1	10.8
$^{131}_{53}$J	0.36	23.4	11.3
$^{51}_{24}$Cr	0.32	26.5	12.1
$^{203}_{80}$Hg	0.28	28.7	12.6
$^{141}_{58}$Ce	0.145	51.6	16.9
$^{170}_{69}$Tm	0.084	88.8	22.2

Table I: Measured relative variances v_Q in pulse height and relative half widths w.

The relative variances of the photopeaks of the nuclides listed in table I, were measured as indicated and the results were plotted in fig. IV–2. The points of fig. IV–2 were fitted to a straight line according to the method of least squares, from which the constants α and β and their standard deviations were calculated:

$$\begin{aligned} \alpha &= (3.2 \pm 0.4) \cdot 10^{-4}, \\ \beta &= (7.403 \pm 0.001) \cdot 10^{-4} \text{ MeV}. \end{aligned} \qquad \text{(IV–9)}$$

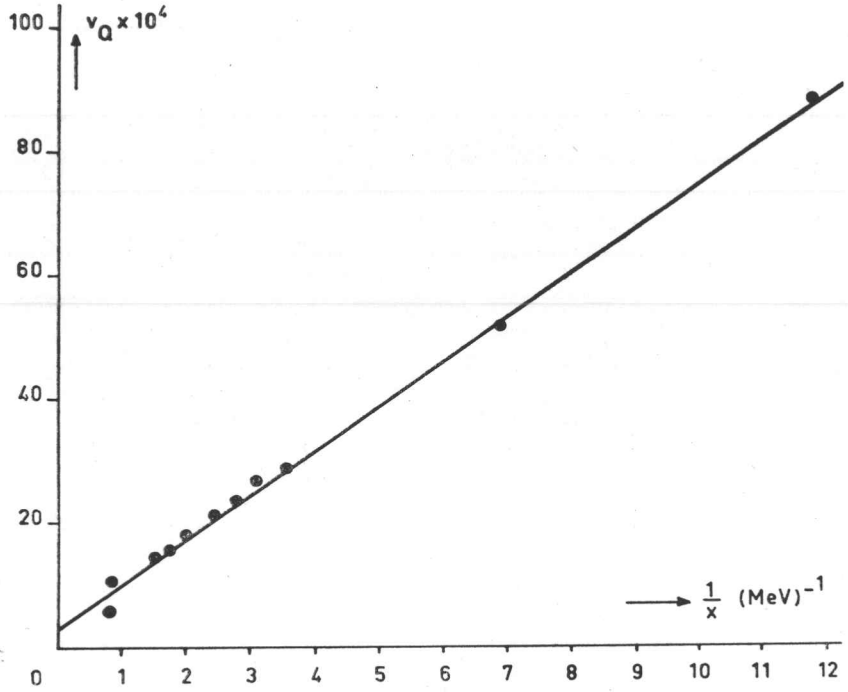

Fig. IV–2. Linear regression of the relative variance v_Q and the inverse mean energy.

Experiments of Bisi and Zappa (1958) indicate that at energies higher than 0.8 MeV the measured values of the relative variance v_Q are lower than the values predicted by IV–5. This is not clearly seen from fig. IV–2, although the trend may be present. This phenomenon may be explained as follows. As has been mentioned before, a photoelectric event and a compton scattering followed by photoelectric absorption of the scattered photon yield the same pulse height. However, while in the first case the pulse is formed by a photoelectron of energy x, in the second case the pulse is formed by a compton electron with energy x_1 and a photoelectron with energy $x_2 = x - x_1$. Both scintillations occurring in different regions of the crystal, they may be assumed as being statistically independent, the resulting relative variance v being given by

$$v(x_1+x_2)^2 = v_1 x_1^2 + v_2 x_2^2 \qquad \text{(IV–10)}$$

Equations IV–5 and IV–10 yield for the relative variance

$$v_Q = \alpha \left\{ 1 - \frac{2x_1x_2}{(x_1 + x_2)^2} \right\} + \frac{\beta}{x_1 + x_2} \qquad \text{(IV–11)}$$

which apparently is smaller than the relative variance in pulse height, due to the absorption of an electron with energy $x_1 + x_2$. This being true, the higher energy points must be left out of the least square calculation. However, since repeated calculation without those points showed that the new values of the constants α and β are within the given accuracies equal to those given by IV–9, and since the corrections are to be applied only in an energy range <0.66 MeV, the values given by IV–9 are used for the calculation of the matrix **N**.

The normalisation factor C in equation III–15 is given by

$$\int_{-\infty}^{+\infty} N(E,x)dE = 1 \qquad \text{(IV–12)}$$

which yields

$$C_1 = x_1 \sqrt{2\pi v_Q x_1} \qquad \text{(IV–13)}$$

4. THE SOLUTION OF THE RESOLUTION EQUATION

To carry out the resolution correction on the measured pulse height distributions described in chapter II a matrix **N** was constructed from the function $N(E,x)$ given by equation III–15. The pulse height spectra arisen from scattering of ^{137}Cs gamma rays were measured in 30 channels, each channel width being approximately equal to 0.02 MeV, in an energy range between 0.08 MeV and 0.66 MeV. Therefore the matrix **N** was calculated for $E_n = x_n = 0.66$ MeV with $\Delta x = 0.02$ MeV. To calculate the matrix elements the NBS probability function tables (1953) were used, the values of the relative variance being calculated from equation IV–5.

To get an idea of the condition of the matrix **N** in solving the set of linear equations IV–1 its determinant (calculated on the X–1 digital computor of the 'Mathematisch Centrum' in Amsterdam) can be weighed against the diagonal element product. The ratio of this determinant to the

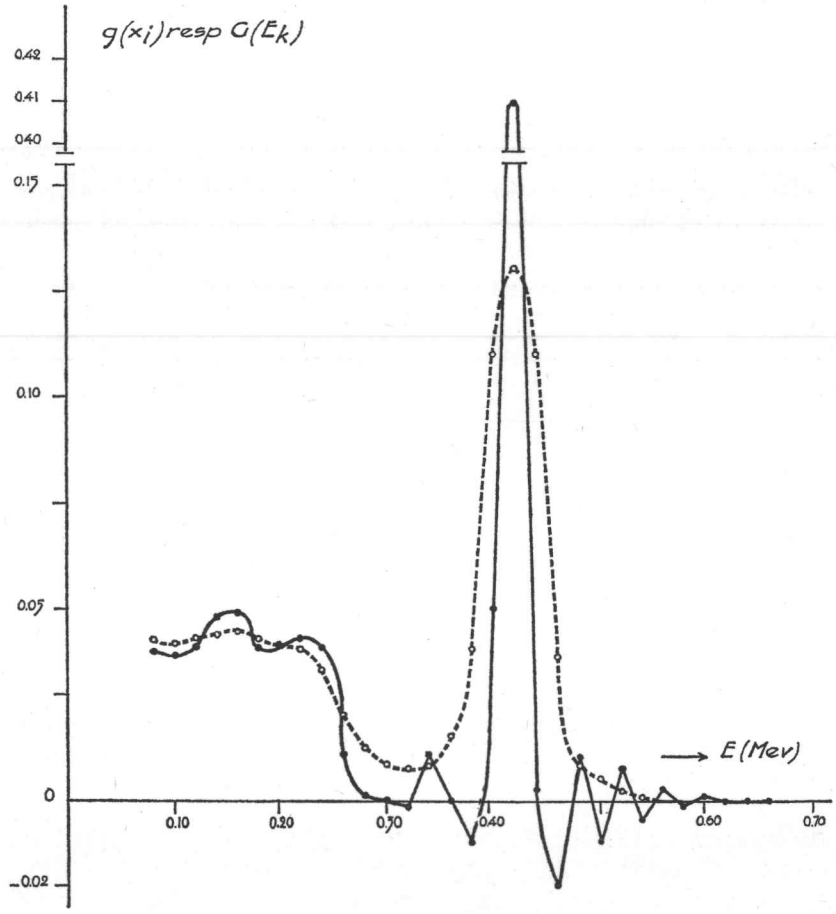

Fig. IV–3. The solution $g(x_1)$ (drawn line) of the resolution matrix equation III–1 compared with the measured pulse height distribution (dashed line), of ^{198}Au.

diagonal element product being about 10^{-6}, the condition of the matrix **N** might not be very good.

To examine the physical importance of this mathematical difficulty, the matrix was inverted and applied to a pulse height spectrum of mono-energetic photons, the calculations being carried out on the X–1 digital computor. In fig. IV–3 a pulse height spectrum of ^{198}Au, which is 'sharpened' by this procedure, is shown.

Though the 'sharpening action' of this method is clearly demonstrated, it is obvious from the occuring oscillations that the solution method cannot be correct. Other solution methods, such as the iterative procedure proposed by Freedman *et al* (1956), which have been used by Villforth *et al* (1958) in the resolution correction in X-ray spectrometry and by Skargard *et al* (1961), meet with the same difficulties (as already mentioned by Villforth and collaborators). These difficulties can be explained from the bad condition of the matrix **N**, which is due to the divergence of the approximating 'solution' (see chapter III), even called a 'pseudo solution' by Dixon and Aitken (1958).

To obtain a function which, within the mentioned restriction, represents as good as possible the true electron energy distribution $g(x)$, some 'trial and error' method seems to be unavoidable. Such a method was applied in this work: from the solution obtained by matrix inversion a set of numbers was averaged. This set, forming a vector $\mathbf{g}'$, is multiplied with the resolution matrix **N**. From this result a correction for the vector $\mathbf{g}'$ can be estimated which, applied to this vector, yields a more approximating vector $\mathbf{g}''$. This new vector was remultiplied with the matrix **N** and again corrected. This procedure was repeated until the finally corrected vector $\mathbf{g}^{(n)}$, when multiplied with the matrix **N**, fits with the measurements within a reasonable accuracy. As can be demonstrated with fig. V–8 in chapter V, this 'trial and error' method can be used with quite satisfactory results.

CHAPTER V

The escape correction

1. INTRODUCTION

As has been stated in chapter III, the absorption of the incident photon energy in a scintillation crystal is not complete, part of the photon energy escaping from the crystal. These escape effects are due to the various ionization processes that occur in the scintillation material. In the first place not all of the incident photons do interact with the crystal material, the probability of interaction being described by the total efficiency factor $\varepsilon(E')$. Furthermore, if photoelectric interactions take place, fluorescent radiation may be emitted, which fluorescent radiation can either be absorbed in the crystal or escape from the crystal. In the latter event, part of the interacting photon energy – which part is equal to the characteristic X-ray of the scintillating material, in this thesis considered as being only that of iodine – is not converted into electronic motion, as a result of which an X-ray escape peak will appear in the spectrum. Finally, if compton interactions take place, part of the interacting photon energy is scattered, the remaining being converted into electronic motion. The scattered photons either escape from the crystal or again interact with the crystal material. The first event causes an electron kinetic energy distribution that can be calculated exactly, while the latter event either results in an increased photopeak if the secondary interaction involves photoelectric absorption, or changes the shape of the compton continuum if the multiple scattered photons escape from the crystal.

As has been argued in section III.4, the correction for these escape-effects in the detector crystal can be carried out, in an arbitrarily close approximation, approximating the solution of the Volterra integral equation III–17 by matrix inversion. The kernel of this integral equation is composed of three terms (see equation III–13), each of them being multiplied to the total efficiency factor $\varepsilon(E')$. The first of these terms describes the probability of the occurrence of an electron kinetic energy $x = E'$, either by primary or by secondary photoelectric effect. The second term gives the probability of the occurrence of an electron kinetic energy $x = E' - \Phi$, describing the effect of X-ray escape. The third term $X(x,E')$

describes photon escape after compton interactions. These factors and terms being quantitatively known, a matrix can be constructed from the kernel, with the aid of which an approximation to the solution of equation III–17 can be obtained. Such a matrix and its inverse will be given in table VI at the end of this paper. It can be used for escape corrections on measurements in comparable geometries, provided that

a. the pulse height spectra are already corrected for the limited resolution (see chapter IV) and
b. the used NaI/Tl scintillation crystal has a diameter, equal to its thickness, of $^3/_4$ inch.

In the sections V.2 to V.6 the evaluation of the various quantities composing the kernel $\varepsilon(E')k(x,E')$ is discussed, while the construction of the matrix is described in the sections V.7 and V.8.

2. THE TOTAL EFFICIENCY

The total efficiency $\varepsilon(E')$, as defined in section II.3, in general depends on the geometry of the measuring set-up. While for geometries in which a parallel photon beam is normally incident on the plane side of the crystal $\varepsilon(E')$ can be evaluated quite simply, evaluation of $\varepsilon(E')$ for geometries in which photons are incident from all directions is very tedious, the probability of interaction of a photon in the crystal depending on its direction. This dependency vanishes when the crystal can be considered as being isotropic, *i.e.* if the crystal has the dimensions of a sphere.

The total efficiency for a point source on the central axis of the crystal can be calculated according to a graphical method given by Wapstra (1953). Such calculations were carried out for the actual cylindrical crystal and for a spherical crystal with a radius R given by

$$^4/_3\,\pi R^3 = {}^1/_4\,\pi d^3$$

in which d is the diameter, equal to the thickness, of the cylindrical crystal. The calculations were performed for two distances between the source and the front of the crystal. The results of these calculations are compared with each other in table II. The integrations were carried out numerically and the values of μ_0, the total attenuation coefficient in cm^{-1}, were recalculated from the cross sections of NaI, given by Wapstra *et al* (1959).

Photon energy (MeV)	μ_0 (cm^{-1})	4 cm		7 cm		$1-e^{-\mu_0 d}$
		sph.	cyl.	sph.	cyl.	
0.08	10.92	0.904	0.908	0.981	0.983	1
0.15	2.18	0.752	0.755	0.943	0.944	0.984
0.40	0.424	0.418	0.422	0.485	0.487	0.555
0.60	0.299	0.273	0.278	0.342	0.344	0.435

Table II. Comparison of calculated total efficiency factors for spherical resp. cylindrical NaI/Tl crystals at source-crystal distances of resp. 4 cm and 7 cm.

As may be apparent from table II there are no appreciable differences between spherical and cylindrical crystal efficiencies at distances >4 cm for energies <0.15 MeV. At higher energies the error made in the sphere approximation is less than 1% at distances >7 cm and is about 2% at a distance of 4 cm.

A scattering medium can be considered as an assembly of virtual point sources, in which those close to the detector contribute mostly to low energy photons incident on the detector. Therefore a cylindrical crystal in such a geometry may be approximated by a sphere with a reasonable accuracy.

The total efficiency for the measurement of a continuous energy distribution $S(\mathbf{r},E')$ in a point $\mathbf{r}$ within a scattering medium, with the aid of a spherical scintillation crystal located in point $\mathbf{r}$, can be derived as follows (see fig. V–1).

As

$$S(\mathbf{r},E')dE' = dE' \int_{4\pi} \mathbf{N}(\mathbf{r},\mathbf{u},E')du \qquad \text{(V–1)}$$

is the number of photons with energy E' in the range dE' that are incident per unit time on a sphere of unit cross sectional area located in point $\mathbf{r}$,

$$S(\mathbf{r},E')\rho d\rho d\varphi$$

is the number of photons with energy E' in the energy range dE' that are

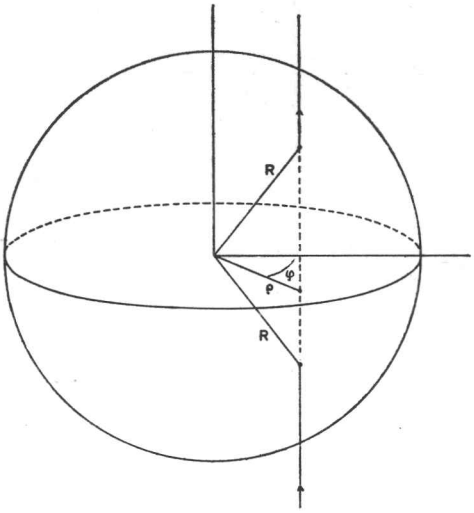

Fig. V–1. Calculation of the total efficiency factor of a spherical crystal.

incident per unit time on a differential area at a distance ρ from the centre of the sphere. If this sphere is a NaI/Tl crystal having a radius R, the pathlength of the differential beam through the crystal is equal to $2\sqrt{R^2-\rho^2}$, the number of photons that have interaction in the crystal being

$$S(\mathbf{r},E')\rho d\rho d\varphi \left\{ 1 - \exp\left(2\mu_0 \sqrt{R^2-\rho^2} \right) \right\}$$

Now the total efficiency $\varepsilon(E')$, according to its definition, can be calculated from

$$\varepsilon(E') = \frac{\int_0^{2\pi} d\varphi \int_0^R \left\{ 1 - \exp\left(2\mu_0 \sqrt{R^2-\rho^2} \right) \right\} \rho d\rho}{\int_0^{2\pi} d\rho \int_0^R \rho d\rho} \qquad \text{(V–2)}$$

which yields

$$\varepsilon(E') = 1 - \frac{1}{2\mu_0^2 R^2}\{(2\mu_0 R + 1)e^{-2\mu_0 R}\} \qquad \text{(V–3)}$$

This formula is better adapted to the conditions of measurement than is formula III–2. Strictly speaking the latter is only valid for monodirectional parallel beams. Since the difference between those two formulae cannot be neglected (see fig. V–2), in evaluating the escape-matrix formula V–3 was used for calculations of the total efficiency $\varepsilon(E')$.

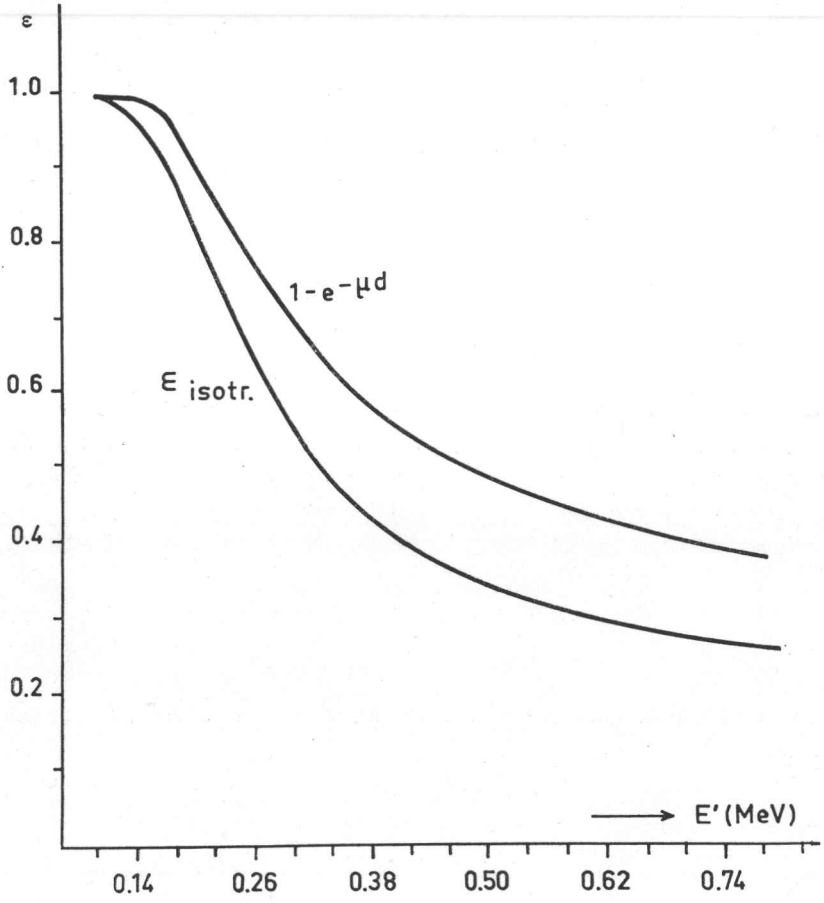

Fig. V–2. Calculated total efficiency factors of an isotropic NaI/Tl crystal compared with calculated total efficiency factors of a cylindrical NaI/Tl crystal for a monodirectional beam incident normally on a flat side of the crystal.

The total efficiency may be influenced by attenuation effects in the coating material of the crystal. The crystal was coated with a 3.9 mm layer of aluminium and the crystal-photomultiplier assembly was partly enveloped in a polythene tube with a wall thickness of 1.5 mm. The attenuation of these layers is negligible.

3. THE PHOTOPEAK EFFICIENCY

The photopeak efficiency, as defined in section III.3, also depends in general upon the geometry of the measuring set up. This is only true if secondary absorption contributes to the photopeak. If secondary absorption in the crystal is negligible, the photopeak efficiency is given by

$$p = \frac{\tau}{\mu_t} \qquad \text{(V–4)}$$

in which τ is the photoelectric attenuation coefficient and μ_t is the total attenuation coefficient which, in this case, is equal to the sum of the photoelectric and the compton attenuation coefficient. However, as has been argued before, a crystal having such dimensions that secondary absorption is negligible, is unfavourable for use in a scintillation spectrometer for reasons concerning both the total efficiency and spureous effects as backscatter against the photomultiplier window.

Secondary (and higher order) interactions consist of compton scattering after compton scattering and photoelectric absorption after compton scattering. While the first type of higher order interactions only affects the compton continuum (see section V.7), the latter type contributes to the photopeak, as a result of which the photopeak efficiency increases. As the escape of scattered photons depends on where the scattering event is located in the crystal, which in turn depends on the geometry of the measuring set-up, the ratio between these two types of higher order interactions, and accordingly the photopeak efficiency, also depends upon the geometry of the measuring set-up.

Therefore experimental determination of the photopeak efficiency, which can be done by determining the ratio of the area of the photopeak to the area of the spectrum, must be adapted to the measuring conditions described in chapter II.

To carry out such an experimental determination, the monoenergetic pulse height spectra of 4 nuclides (see table III) were measured in three different geometries:

a. the source located along the central axis of the scintillation detector at a distance >15 cm from the centre of the crystal;
b. the source located along the diagonal of the longitudinal cross section of the crystal, also at a distance >15 cm from the centre of the crystal;
c. the source located along an axis through the centre of the crystal parallel to its flat sides, also at a distance >15 cm from the centre of the crystal.

In these geometries approximate parallel beams are incident on the whole crystal. The area ratios were determined by copying the measured spectrum on a sheet of grade 1 chromatographic paper, cutting out the spectrum and weighing the photopeak and the spectrum separately. The results of these experimental determinations are given in table III.

Nuclide	Gamma ray energy (MeV)	p			
		a	b	c	mean
$^{137}_{55}Cs$	0.66	0.207	0.204	0.192	0.20
$^{198}_{79}Au$	0.41	0.318	0.306	0.311	0.31
$^{51}_{24}Cr$	0.32	0.412	0.406	0.404	0.41
$^{203}_{80}Hg$	0.28	0.483	0.476	0.490	0.48

Table III. Experimentally determined photopeak efficiencies in three different geometries: a. a source on the central axis of the detector, b. a source on the diagonal axis of the crystal, and c. a source on the horizontal axis through the centre of the crystal. All measuring distances were larger than 15 cm.

As may follow from table III the maximum deviation from the mean caused by variation of the direction of incidence is about 2%. This being within the accuracy of the spectrometric measurements, the given mean

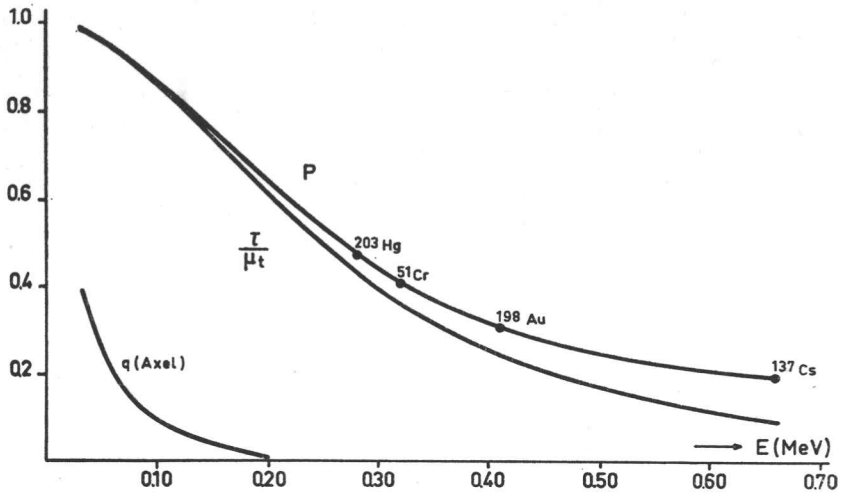

Fig. V–3. The photopeak efficiency p with the relative probability $\frac{\tau}{\mu_t}$ of photoelectric interaction, both as a function of the incident photon energy.
q is the X-ray escape probability for 'very poor geometry' according to Axel (1953).

values can be used for interpolating the values of p. To this purpose the mean values of p, given in table III, were plotted as a function of the incident energy in fig. V–3. For comparison a curve of p, calculated according to equation V–4, is also given.

4 THE X-RAY ESCAPE

As has been mentioned in section II.1, fluorescent X-radiation following photoelectric absorption can escape from the crystal, as a result of which the crystal does not absorb the energy corresponding to the characteristic X-ray energy of the scintillation material, assumed to be equal to 0.033 MeV.

In contrast with the problem of the previous section, the probability of X-ray escape is difficult to determine experimentally, the X-ray escape peak being separated from the photopeak at low energies only. To demonstrate this, fig. V–4 shows the pulse height spectra of ^{141}Ce (γ-energy 0.145 MeV) and ^{170}Tm (γ-energy 0.084 MeV). In the case of ^{141}Ce

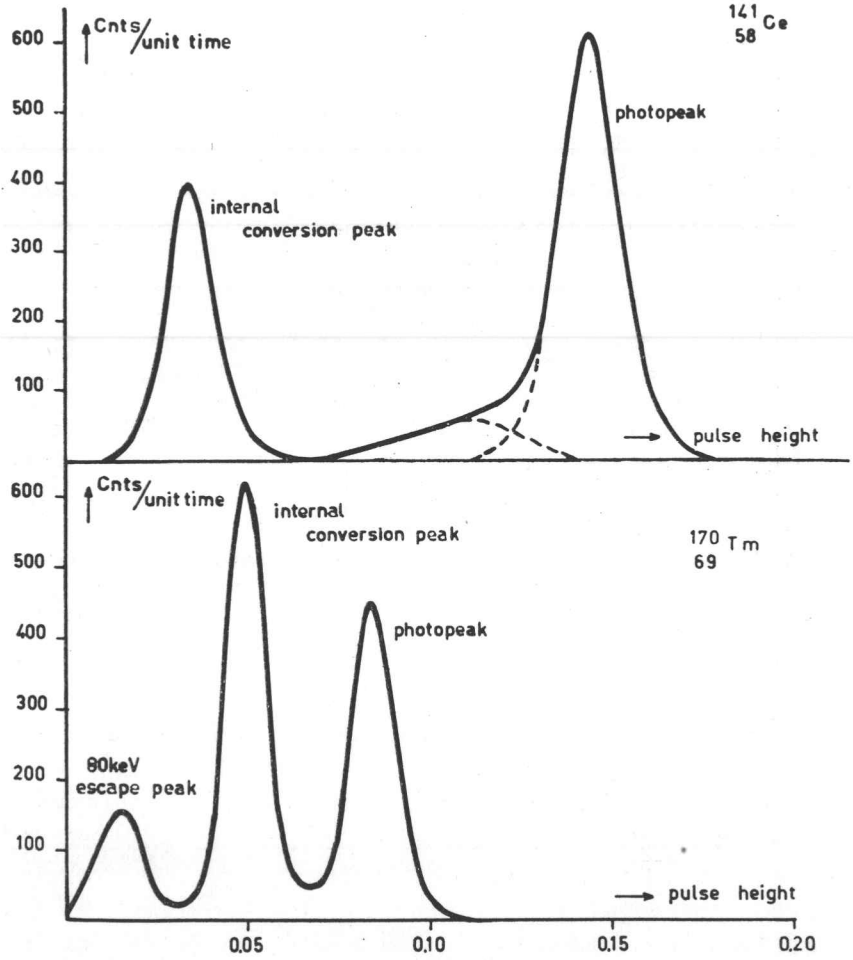

Fig. V–4. Pulse height distributions of ^{141}Ce and ^{170}Tm. Dashed line: extrapolated X-ray escape peak.

the escape peak can be resolved from the photopeak (dashed line in the figure) by making use of the gaussian shape of the peaks. In the case of ^{170}Tm only the escape peak of the internal conversion radiation (about 0.05 MeV) is demonstrable, the escape peak of the primary gamma radiation being incorporated completely in the internal conversion peak. Internal conversion causes difficulties in many of the low energy gamma-

emitters. Furthermore, as Axel (1953) has already noted, experimental determination of the escape probability at energies slightly above the K binding energy of iodine is extremely difficult.

Assuming that some approximations can be made, it is easier to calculate the X-ray escape probability *i.e.* the ratio q of the escape peak to the involved photopeak (see section III.3), as indicated by Axel (1953). The approximation of isotropicity, described in the previous sections, *i.e.* considering the crystal as a sphere with a finite radius R, however, leads to a very complicated expression for q, which expression is extremely difficult to evaluate. Axel pointed out that for the low energies involved the crystal may be considered as infinitely thick, the X-ray escape only occurring after photoelectric absorption near the edges of the crystal. So if it is assumed that every photon with energy < 0.2 MeV 'sees' the crystal as infinitely thick, no matter at what edge it is penetrating, the calculated values of Axel may be used. As for measurements in a scattering medium, it seems reasonable to use Axel's values of q for 'very poor geometry', *i.e.* a geometry where the source is in contact with the crystal. These values are plotted in fig. V–3.

5. THE ESCAPE OF SCATTERED PHOTONS

The escape of scattered photons, as already is set forth above, is described by a function $X(x,E')$, such that $X(x,E')dx$ is the probability that after one or more compton interactions and escape of the scattered photons an electron kinetic energy x in the range dx will be produced.

Multiple interactions in the crystal influence the function $X(x,E')$. These multiple interactions can be distinguished in two groups:

a. those in which a compton process is followed by photoelectric absorption of the scattered photon energy;
b. those in which a compton process is followed by compton interactions, resulting in the escape of (multiple) scattered photons.

Assuming that no multiple interactions take place or that multiple interactions consist only of those mentioned in group a., the function $X(x,E')$ can be derived from the Klein Nishina differential cross section for compton scattering (Heitler, 1954; Loevinger, 1956), which derivation yields

$$0 \leqslant x \leqslant x_{max}: X(x,E') = \frac{1}{B} \cdot \frac{1}{E'^2} \left\{ 2 + x \frac{x(E'+1)^2 - E'(2E'+x^2)}{E'^2(E'-x)^2} \right\}$$

$$x > x_{max}: X(x,E') = 0 \qquad \text{(V-5)}$$

in which $x_{max} = 2E'^2/(1+2E')$ is the maximum recoil electron energy as follows from the laws of conservation of energy and momentum, and B is a normalisation constant, given by

$$\int_0^{x_{max}} X(x,E')dx = 1 \qquad \text{(V-6)}$$

In the equations V-5 and V-6 x as well as E' are expressed in units m_0c^2.

When multiple interactions are neglected or restricted to group a., an analytic evaluation of the matrix elements from the equations III-13, V-3 and V-5 can be carried out. The usefulness of this analytically evaluated matrix, in other words the justification of the applied approximation, can only be experimentally tested. Such experiments are described in section V.7.

6. BACKSCATTER

Backscatter against parts of the photomultiplier causes spurious peaks in the measured pulse height distributions. Lidén *et al* (1954) have proposed a correction method, which is very tedious and not very adequate to use in measuring geometries as regarded here.

If a narrow parallel beam is incident along the axis of the photomultiplier, backscatter (mainly against the photomultiplier window) is about 40% larger than if a narrow parallel beam is directed parallel to the photomultiplier window. Hence, experimental determination of the backscatter correction must be adapted as much as possible to the actual measuring geometry.

For this purpose a 'point'-source of the nuclides ^{137}Cs, ^{122}Sb, ^{103}Ru and ^{198}Au was placed at a distance of about 4 cm from the centre of the crystal:

a. along the axis of the photomultiplier;
b. along the diagonal of the crystal, and
c. along a line through the centre of the crystal parallel to the photomultiplier window.

In these arrangements practically all parts of the crystal receive radiation from the source, the directions of incidence however being different in the three geometries.

From these measurements the ratio of the backscatter peak to the photopeak was determined. The maximum difference between the ratios found in the different geometries was less than 8%. In fig. V–5 these ratios, averaged over the three geometries, are given as a function of the incident energy.

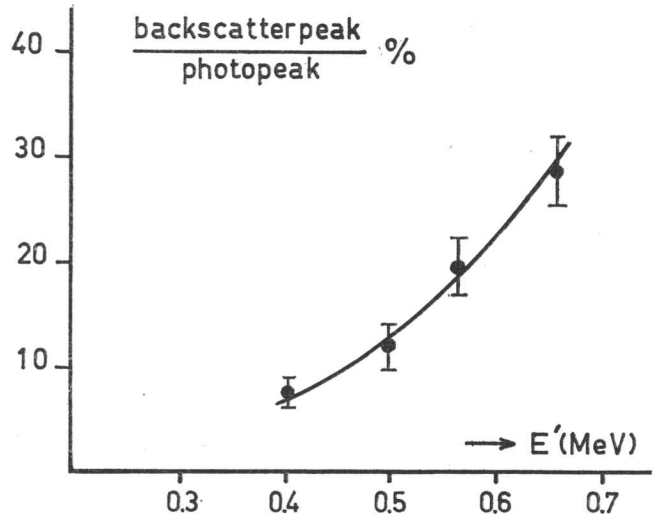

Fig. V–5. Measured backscatter/photopeak ratios as a function of the incident photon energy.

Great care was taken to eliminate the backscatter from the environment, the measurements being carried out with the source and the detector at least at 2 m from the nearest substantial obstacle.

These measurements were used to add a backscatter correction to the escape matrix (see section V.8).

7. MULTIPLE SCATTERING IN THE CRYSTAL

Multiple interactions of the type in which compton interaction is followed again by compton interaction resulting in the escape of the multiple scattered photon, may change the compton continuum in respect to a compton continuum that would result from single events in the crystal. If this type of multiple interactions cannot be neglected, the analytical procedure for the evaluation of the escape matrix, described in section V–5, can no longer be used.

As has been stated before, the occurrence of this type of multiple interaction can be tested experimentally only. This can be done easily, for a monoenergetic energy distribution being represented by

$$S(E')dE' = \delta(E' - E')dE' \tag{V–7}$$

causes a recoil electron energy distribution, given by

$$g(x) = \int_{x}^{E_0'} \varepsilon(E')k(x,E')\delta(E' - E_0')dE' = \varepsilon(E_0')k(x,E_0') \tag{V–8}$$

This electron energy distribution yields a pulse height distribution:

$$G(E) = \int_{0}^{E_0'} N(E,x)\varepsilon(E_0')k(x,E_0')dx \tag{V–9}$$

which can be approximated by

$$G(E_k) = \Delta x \sum_{i=1}^{n} N(E_k,x_i)\varepsilon(E_0')k(x_i,E_0') \tag{V–10}$$

in which the vector $\varepsilon(E_0')k(x_i,E_0')$ is obtained from

$$\varepsilon(E_0')k(x_i,E_0') = \varepsilon(E_0') \int_{x_i-\frac{1}{2}\Delta x}^{x_i+\frac{1}{2}\Delta x} k(x,E_0')dx \tag{V–11}$$

If multiple interactions of the type described are negligible, the pulse height distribution calculated according to the described procedure, must fit with a measured pulse height distribution.

This check was done by calculating the pulse height distribution of the nuclides ^{137}Cs and ^{189}Au according to the described procedure (normalized to one *interacting* photon per unit time, *i.e.* $\varepsilon(E_0') = 1$, and comparing

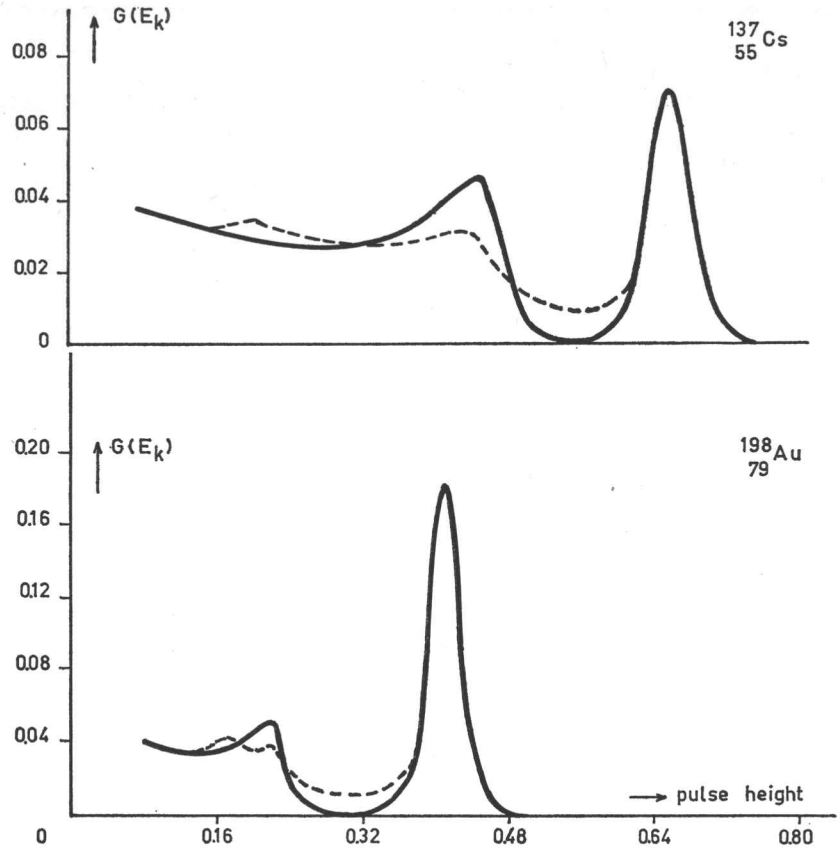

Fig. V–6. Comparison of calculated (drawn line) and measured (dashed line) pulse height spectra, resp. of ^{137}Cs and ^{198}Au.

them with measured pulse height distributions of these nuclides. The measurements were normalized in such a way that the area of the measured photopeak became equal to the area of the calculated photopeak.

As will be seen from fig. V–6, the measured pulse height distributions, compared with the calculated distributions, show an 'additional spreading' at the edge of the compton continuum. Using the analytically derived matrix described in section V.5 the error made at energies just below the compton edge can reach values as large as 30 % in respect to the maximum calculated value in the compton region. In the energy range above the compton edge the error is hardly smaller, in the case of ^{198}Au even larger.

Hence this error cannot be left unconsidered. As it is likely that as a result of multiple interactions of the type described above, the energy of the recoil electrons shifts to higher values, the observed 'additional spreading' may be explained by the occurrence of this type of multiple interactions in the crystal to such an extent that it cannot be neglected.

A theoretical treatment of the problem of multiple scattering in the crystal being almost impossible, an experimental method must be found to modify the escape matrix in such a way, that the error made in the escape correction is as small as possible. Such an experimental method is described in section V.8, the final construction of the escape matrix being carried out with the aid of an interpolation carpet (Yates, 1946).

8. THE FINAL CONSTRUCTION OF THE ESCAPE MATRIX

To approximate the solution of the Volterra integral equation III–17 a matrix must be constructed from its kernel. Obviously this matrix will be a triangular matrix, the rows of which can be considered as the electron energy distributions, resulting from incident monoenergetic photons with the corresponding energy E' (see table VI). The diagonal elements of this matrix represent the probability of an electron kinetic energy $x = E'$, resulting from a complete absorption of the incident photon energy. Numerically these elements are equal to the photopeak efficiency $p(E_j')$ multiplied to the total efficiency factor $\varepsilon(E_j')$, in wich $p(E_j')$ is determined experimentally according to section V.3, and $\varepsilon(E_j')$ is calculated according to formula V–3.

In the low energy range ($E' < 0.2$ MeV) the remaining elements of the matrix are determined by the X-ray escape probability $q(E_j')$. A difficulty arises here in the evaluation of the concerned delta function, the energy of recoil electrons after escape of the fluorescent X-ray being 0.033 MeV lower than the initial photon energy. As, however, in measurements of continuous photon energy distributions the photon energy is only discriminated in intervals of 0.02 MeV, each photon energy interval can be split in two parts, so that each part correspondingly contributes to a different interval lower down.

In the higher energy range ($E' > 0.2$ MeV) the non diagonal elements are determined by compton scattered photon escape, expressed in the function $X(x,E')$, which function represents the probability of a recoil electron energy x in the range dx. As is demonstrated in the previous

section this function cannot be evaluated with the aid of the Klein Nishina differential cross section for compton scattering, because of the occurrence of multiple scattering in the crystal. An experimental method to modify the function $X(x,E')$ in such a way that the error made in the escape correction is as small as possible, may be the following (Yates, 1946).

The function $X(x,E')$ can be considered as a function $z = f(x,y)$ of the two independent variables x and y. Such a function can be plotted in a three dimensional coordinate system. Then orthogonal projection on the ZOX-plane yields the group of functions $z = f(x)_y$. Now if instead of orthogonal projection, the projection on the ZOX-plane is done according to a certain angle φ with the Y-axis, the same functions $z = f(x)_y$ are imaged on the ZOX-plane, but in this case shifted over a distance $y \cdot \mathrm{tg}\,\varphi$ to the origin. When in this image the points with equal values of x are joined, the joining lines represent the functions $z = f(y)_x$. In this image, a so called carpet (Yates, 1946), the values of $f(x_1)_{y_j}$ and $f(y_j)_{x_i}$ can be interpolated, if the functions are not too complicated and the value of $\mathrm{tg}\,\varphi$ is sensibly chosen.

Now assuming that from a limited number of measured pulse height distributions of monoenergetic nuclides the corresponding electron energy distributions can be determined with a reasonable accuracy, the resulting values for $X(x,E')$ can be plotted in a carpet, as described above, from which the desired values of the elements $X(x_i,E_j')$ may be interpolated.

Sources of the nuclides ^{137}Cs, ^{122}Sb, ^{103}Ru, ^{198}Au, ^{51}Cr, and ^{203}Hg were placed at distances >15 cm from the scintillation detector and the pulse height distributions were measured within a statistical error of less than 0.3 % These pulse height distributions were used in solving the set of linear equations IV–1 (see chapter IV) by matrix inversion. The resulting solutions were plotted and the best approximation to the electron energy distributions $g(x)$ $(=k(x,E_0'))$ was determined by 'trial and error', as described in chapter IV.

An example of this plotting is given in fig. V–7, in which the drawn line represents the obtained best approximation. A comparison of the final result, multiplied by the matrix **N**, with the measured spectrum is given in fig. V–8.

The dashed line in fig. IV–7 shows the function $X(x,E')$ analytically determined according to section V.5. As will be apparent, multiple scattering in the crystal does not change the compton continuum in the lower energy range.

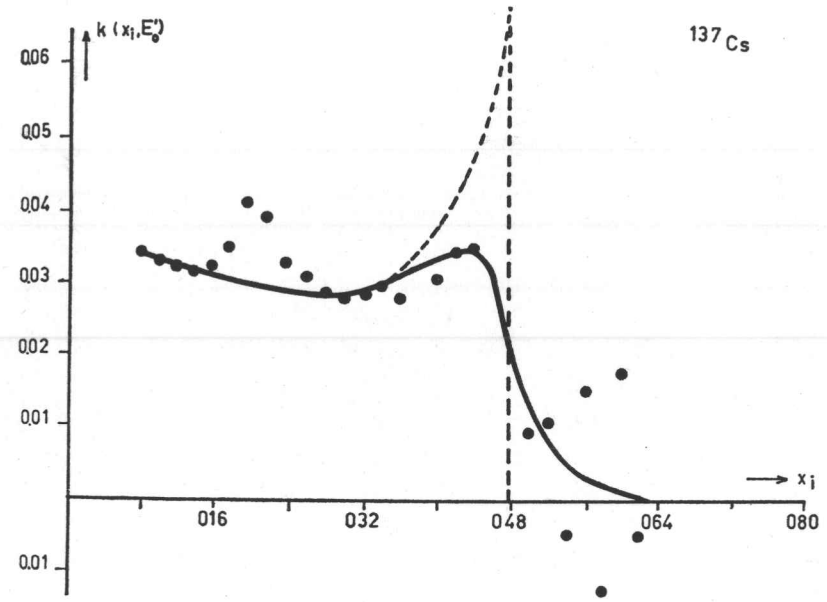

Fig. V–7. Solution of the resolution matrix equation III–1 (dots), the best approximation to the electron energy distribution (drawn line), and the analytically determined compton electron energy distribution (dashed line).
For the sake of clarity, the line representing the photopeak is omitted.

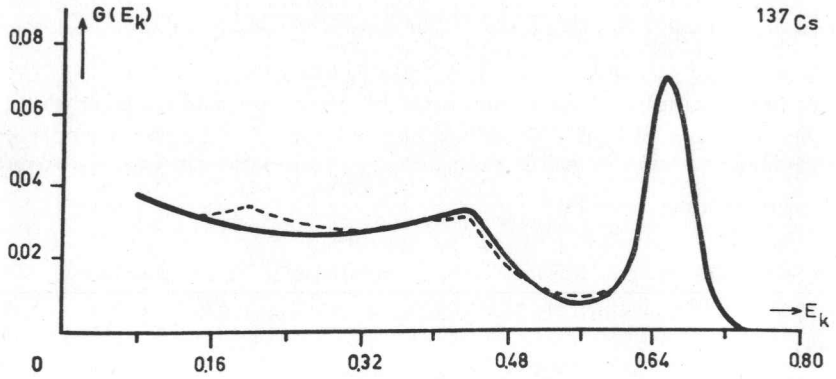

Fig. V–8. Comparison of the calculated (drawn line) and the measured (dashed line) pulse height distribution of ^{137}Cs, the calculation including multiple effects in the crystal.

From the six functions $X(x,E')$, determined experimentally according to the method described above, a carpet was constructed, a schematic representation of which is shown in fig. V–9. From such a carpet the non diagonal elements that are different from those which can be calculated analytically, were interpolated.

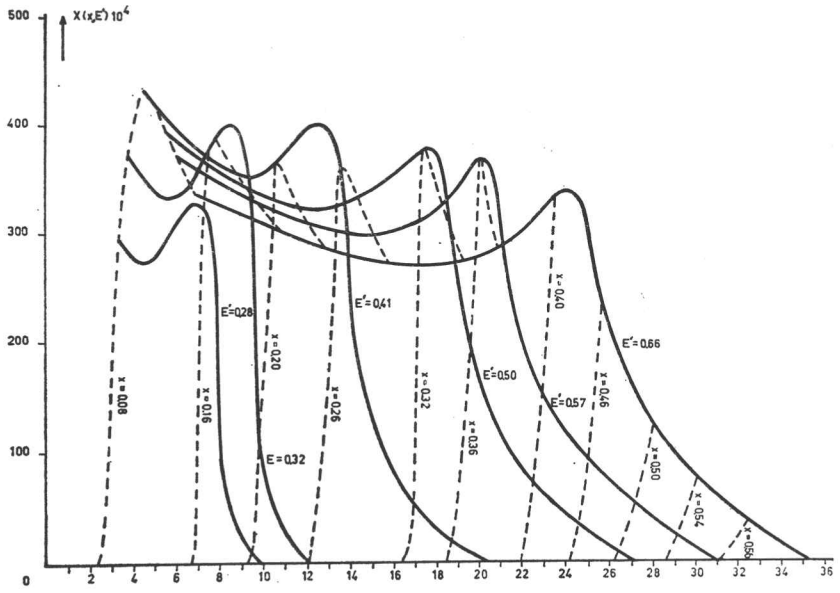

Fig. V–9. Interpolation carpet to determine the elements of the escape matrix.

The backscatter measurements, described in section IV.6, yielded a backscatter correction which was added to the matrix elements involved.

Accordingly an escape matrix of the order of 30 in the energy range between 0.08 MeV and 0.66 MeV was constructed. The inverse of this matrix can be applied directly to resolution corrected pulse height distributions to yield an approximation of the incident photon energy distributions. The matrix and its inverse are given in table VI at the end of this thesis and can be used for correcting backscatter and escape effects in a scintillation detector in which a NaI/Tl crystal of $^3/_4$ inch diameter and $^3/_4$ inch thickness is coupled directly to a photomultiplier window, having a diameter of 1 inch.

CHAPTER VI

Experimentally determined photon energy distributions in a cylindrical water medium

1. THE CORRECTION OF THE PULSE HEIGHT SPECTRA

The pulse height spectra, measured as described in chapter II, were first sharpened according to the method described in chapter IV, yielding an approximation of the electron energy distribution $g(x)$ within the scintillation crystal. The resulting approximations of $g(x)$ are given in fig. VI–1.

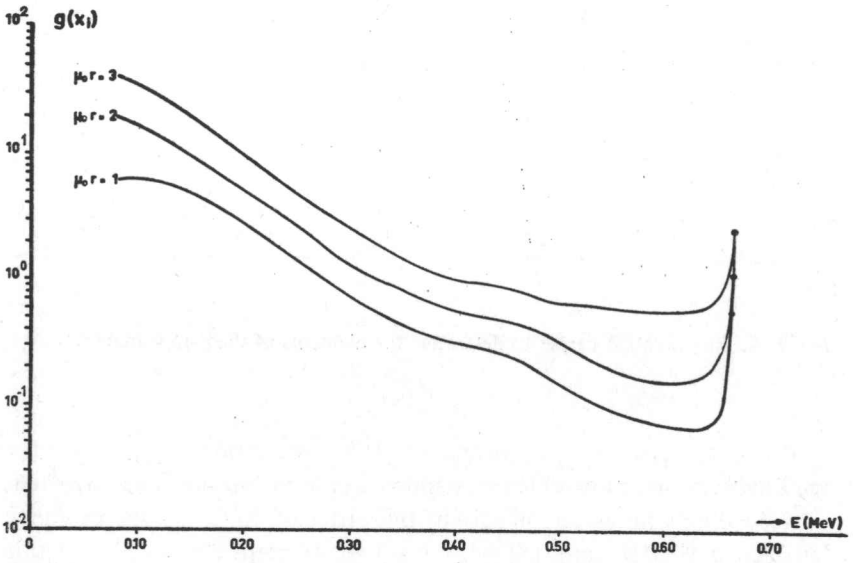

Fig. VI–1. Electron energy distributions within the NaI/Tl crystal, generated by scattered photons in a cylindrical water medium with point isotropic source geometry at three penetration distances.

As has been described in chapter III, an incident continuous spectrum $S(E')$ causes an electron energy distribution in the scintillation crystal,

given by

$$g(x) = \int_{x}^{E_0'} \varepsilon(E')k(x,E')S(E')dE' \qquad \text{(III–17)}$$

The incident spectrum $S(E')$ can be considered as the sum of two components, one of which giving the contribution of the unscattered photons, and the other giving the contribution of the photons scattered at least once. For a point isotropic source geometry, $S(E')$ can be written as

$$S(E') = \frac{e^{-\mu_0 r}}{4\pi r^2}\delta(E' - E_0') + S_s(E') \qquad \text{(VI–1)}$$

in which $S_s(E')$ is the 'scattering component'.

Substituting VI–1 into III–17, we obtain

$$g(x) = \frac{e^{-\mu_0 r}}{4\pi r^2}\varepsilon(E_0')k(x,E_0') + \int_{x}^{E_0'} \varepsilon(E')k(x,E')S_s(E')dE' \qquad \text{(VI–2)}$$

An approximation to the solutions $S_s(E')$ of VI–2 can be obtained by writing:

$$g(E_i) - \frac{e^{-\mu_0 r}}{4\pi r^2}\varepsilon(E_0)k(E_i,E_0) = \Delta E \sum_{j=i}^{h} \mathbf{A}_{i,j} S_s(E_j) \qquad \text{(VI–3)}$$

in which $\mathbf{A}_{i,j}$ is the matrix formed by the elements $\varepsilon(E_j)k(E_i,E_j)$ and given in table VIa.

The set of equations VI–3 yields:

$$4\pi r^2 e^{\mu_0 r} S_s(E_j)\Delta E = \sum_{j=i}^{h} \mathbf{A}^{-1}{}_{i,j}\{4\pi r^2 e^{\mu_0 r} g(E_i) - \varepsilon(E_0)k(E_i,E_0)\} \qquad \text{(VI–4)}$$

in which $\mathbf{A}^{-1}{}_{i,j}$ is the inverse matrix, given in table VIb.

Accordingly, the vectors $g(E_i)$ were first multiplied by a factor $4\pi r^2 e^{\mu_0 r}$, and then the electron energy distribution, resulting from the unscattered photons, *i.e.* $k(E_i,E_0')$, were subtracted out. From these so corrected

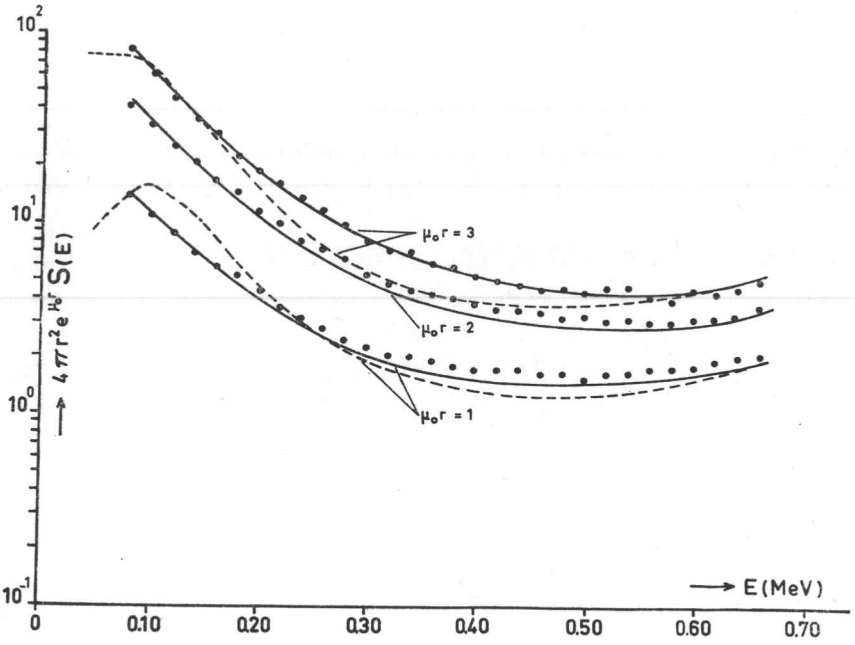

Fig. VI–2. Photon energy distributions within a cylindrical water medium with point isotropic source geometry at three penetration distances. Dots indicate the measured values in the present experiments. Drawn lines indicate photon energy distributions calculated according to the moment method (Goldstein and Wilkins). Dashed lines indicate photon energy distributions measured bij Theus and collaborators and adapted to the present scale.

vectors, the vectors $4\pi r^2 e^{\mu_0 r} S_s(E_j)$ were solved by matrix inversion. The resulting photon energy distributions are given in fig. VI–2.

The drawn lines in the figure represent the scattered photon energy distributions, interpolated for 0.66 MeV primary gamma rays from the calculated data of Goldstein and Wilkins (1954). As will be seen, the agreement is quite reasonable. The dashed lines in the figure show the experimental results of Theus *et al* (1955).

2. BUILDUP FACTORS

Buildup factors with respect to an operator $D(\ ) = \int f(E)dudE$ as defined in section I.3, are generally given by

$$B_f = \frac{\int f(E)S(E)dE}{\int f(E)S_0(E)dE} \tag{I-7}$$

From the measured energy distributions, given in the previous section, three different types of buildup factors were calculated. The first, the *energy buildup factor* B_E, is related to the energy flux at the measuring distance. As the energy flux at energy E in the range dE is given by $ES(E)dE$, the function $f(E)$ in this operator is E. For point isotropic source geometries the energy buildup factor then becomes:

$$B_E = \frac{4\mu r^2 e^{\mu_0 r}}{E_0} \int_0^{E_0} ES(E)dE \tag{VI-5}$$

The second buildup factor is the *energy absorption buildup factor* B_a. This buildup factor is related to the energy absorption in the scattering medium. The number of collisions of photons of energy E in the range dE per unit volume and time is $\mu S(E)dE$. If the average energy which is absorbed after a collision is $\overline{E}$, the energy disposition per unit volume and time by photons of energy E in the range dE is given by:

$$\overline{E}\mu S(E)dE = \mu_a ES(E)dE$$

in which $\mu_a = (\overline{E}/E)\mu$, is the *energy absorption coefficient* at energy E for the medium involved. Hence the function $f(E)$ in this case is $\mu_a E$, and the energy absorption buildup factor for point isotropic source geometries becomes:

$$B_a = \frac{4\pi r^2 e^{\mu_0 r}}{\mu_{a_0} E_0} \int_0^{E_0} \mu_a ES(E)dE \tag{VI-6}$$

The third calculated buildup factor is the *exposure dose buildup factor* B_d, which is related to the dose as measured by an ideal air walled ionization chamber. As the exposure dose is defined in terms of energy

disposition per unit volume of dry air of STP, the exposure dose buildup factor B_d is equal to the energy absorption buildup factor B_a if the scattering medium were air. Accordingly the dose buildup factor becomes:

$$B_d = \frac{4\pi r^2 e^{\mu_0 r}}{\mu_{a_0}' E_0} \int_0^{E_0} \mu_a' E S(E) dE \qquad \text{(VI–7)}$$

in which μ_a' is the energy absorption coefficient of dry air.

In table IV the buildup factors, determined according to the equations VI–5, VI–6 and VI–7 by numerical integration of the measured energy distributions, are compared with values, which are interpolated from the calculated data of Goldstein and Wilkins (1954) and with values measured by Theus *et al* (1955). The values for μ_a and μ_a' are taken from table 2.8 of Morgan's Handbook of Radiology (1955).

	$\mu_0 r = 1$			$\mu_0 r = 2$			$\mu_0 r = 3$		
	B_E	B_a	B_d	B_E	B_a	B_d	B_E	B_a	B_d
Present experiments	2.5	2.4	2.4	4.6	4.4	4.5	7.7	7.1	7.0
Moment method calculations Goldstein *e.a.*	2.4	2.3	2.3	4.5	4.2	4.2	7.7	7.0	7.0
Experiments Theus *e.a.*	2.3						6.4		

Table IV. Comparison of experimental and calculated energy buildup factors (B_E), energy absorption buildup factors (B_a), and exposure dose buildup factors (B_d) at three penetration distances.

3. DISCUSSION OF ACCURACY AND ERRORS

The complexity and the elaborate character of the energy distribution measurements described, obviously imply many potential sources of error. The errors which may occur in the course of different operations

are statistical errors, random and systematic errors, inaccuracies in the approximations, inaccuracies in the interpolations, errors in the machine calculations, and errors in the manual calculations.

By manual operation of the spectrometer, the *statistical errors* in counting can be kept small, provided that the counting time required is small compared to the time in which drift in the electronic equipment becomes important.

Random and systematic errors may occur in measuring the source strengths, in the adjustment of the spectrometer, possibly as a result of random changes in the electronic equipment, and in measuring the penetration distances.

The correction of the measured pulse height spectra is based on an approximate solution of the response equation. Moreover, many factors determining the relation between the pulse height spectra and the incident photon energy distributions were approximations. This may result in *approximation inaccuracies* in the final results.

Errors in the interpolations are probably dominant only in the elements of the 'escape matrix', as most of these elements are interpolated from an experimentally determined carpet (see chapter V).

Errors in the machine calculations, due to machine break down during the operation, and/or to errors in the coding, are very unlikely, for the coding of the data was repeated independently, the second set of coded data serving as a check for the coding as well as for the machine performance.

Apart from the machine calculations about 10^4 hand calculations were carried out. The hand calculated values were checked in several ways, such as comparison on the basis of symmetry in the resolution matrix and random sampled recalculations. Large errors in these values would have been detected easily. Therefore errors of this type in the final results are believed to be negligibly small.

To estimate the ultimate error in the final results, it is convenient to classify the possible sources of error under the following headings:

a. Errors in the pulse height measurements,
b. Errors in the resolution correction, and
c. Errors in the escape corrections.

The pulse height spectra were measured within a statistical error of less than 0.3%. The counting time to obtain this result averaged 1000 sec., during which period the drift in the electronic equipment was found to

be negligible. Random errors may have occurred in the adjustment of the spectrometer. The spectrometer was adjusted in such a way that each setting of the bias potentiometer corresponded to the centre of an energy interval equal to 0.02 MeV, the channel width being adjusted to correspond to that energy interval (chapter II). The maximum error made in these adjustments was about 10% of the channel width. As will be seen from fig. II–8, a drift of the channel over about 10% of the channel width causes errors in the counting rates which do not exceed 2 or 3%.

The accuracy of the normalization of the measured pulse height spectra depends on the error made in measuring the source strengths. These source strengths were measured by comparing the sources with an identical standard source in an ionization chamber. The accuracy of the standard was $\pm$ 2%, and the accuracy of the comparison was about $\pm$ 3%. Hence the source strengths were given within 4% accuracy. Obviously this error, acting as a systematic error, affects the normalized pulse height spectra, and also the finally resulting photon energy distributions, only quantitatively, the normalization factor essentially remaining a constant during all operations.

The accuracy of the resolution correction generally depends upon errors in the elements of the resolution matrix, and upon approximation errors in the solution of the resolution equation (see chapter IV). As the corrected results, obtained finally by trial and error, fitted the original pulse height measurements within 1% when remultiplied to the resolution matrix (see for example fig. V,7), the inaccuracy in the ultimate results is believed to be not greater than the inaccuracy in the measured pulse height spectra.

The escape corrections include a plurality of sources of error. The non diagonal elements of the escape matrix were interpolated from a carpet, which was constructed from experimentally determined electron energy distributions (see section V.8). This implies interpolation errors, which are difficult to estimate. However, it can be shown that relatively large inaccuracies in the non diagonal elements of the matrix only cause slight changes in the corrected results. The experience has been that a fluctuation in the non diagonal elements at some given energy up to 10%, affects the point in the spectrum at the energy involved within less than 1%. So the inaccuracies in the X-ray escape and the backscatter correction as well as interpolation inaccuracies in the compton escape correction, do not affect the final results to a very great extent.

Errors in the diagonal elements of the escape matrix, however, influence the accuracy of the corrected photon energy distribution to a greater extent. These errors are determined by errors in the photopeak efficiency and in the total efficiency factor.

The photopeak efficiencies were determined by interpolation from four experimentally determined values. The experimental determination of the photopeak efficiency was carried out by a weighing method (see section V–2). To this purpose measured monoenergetic pulse height spectra were copied on a sheet of grade 1 chromatographic paper, which has a high grade of homogeneity, and were cut out, whereafter the photopeak and the spectrum were weighed separately. This procedure was repeated 5 times with one spectrum, and the maximum difference found in the weight ratios was less than 1%. The differences due to the dependency upon the direction of incidence (see section V.3) did not exceed 2%, so the measured photopeak efficiencies of the four monoenergetic spectra involved may be considered as accurate within 3%. The interpolation error is believed not to exceed 2%, which is less than the error in the measurements. Generally the photopeak efficiencies are believed to be accurate within 4%.

The diagonal elements are also determined by the total efficiency factor at the energy involved, with which factor the elements of the different rows of the matrix are multiplied. In this factor, which has been calculated from formula V–3 (see section V.2), the dominant type of error apparently is the approximation error. Referring to table II (section V.2), the inaccuracy is estimated to be about 2%. If it is assumed that errors in the attenuation coefficients used are well within this inaccuracy, the error in the diagonal elements amounts to about 6%.

Summarizing the above discussions on possible errors, the measured and corrected photon energy distributions are believed to be accurate within about 10%.

In calculating the buildup factors there may be an additional error due to the fact that the lower energy range ($E<0.08$ MeV) is omitted. Since, however, in this energy range the intensity falls off very rapidly (see ref. Goldstein and Wilkins), this error is believed to be small.

Apart from the mentioned errors there is a possible error of $\pm$ 0.5 cm in adjusting the penetration distances, which distances are taken from the centre of the source to the centre of the scintillation crystal. This error must be taken into account when the results of the measurements are compared with theoretically predicted data.

4. FINAL DISCUSSION

To compare the experimentally determined photon energy distributions with photon energy distributions calculated according to the 'moment method', data of Goldstein and Wilkins (1954) were used to interpolate photon energy distributions at penetration distances of 1, 2 and 3 mean free path lengths with a source energy of 0.66 MeV. In fig. VI–2 the interpolated results are indicated by drawn lines.

As may be apparent from the figure, the experimental photon energy distributions at penetration distances of 1 and 2 mean free path lengths are somewhat higher than the calculated photon energy distributions, the discrepancies, however, remaining mostly within the measuring accuracy. The experimental result at a penetration distance of 3 mean free path lengths is in reasonable agreement with the calculations. Qualitatively the experimental curves show a good similarity with the calculated curves. The small differences can be considered as caused by systematic errors in the measurements as well as in the calculations of Goldstein and Wilkins.

Consequently, as will be seen from table IV, the experimentally obtained buildup factors are in good agreement with buildup factors interpolated from data of Goldstein and Wilkins (1954).

These results can be considered as a mutual confirmation, both for the correctness of the measurements within the measuring accuracy and for the validity of calculations according to the 'moment method' in a geometry as described. Hence, in the experimental set-up, described in chapter II, the cylindrical water medium can be considered as an infinite medium for 0.66 MeV gamma rays.

The dashed lines in fig. VI–2 indicate photon energy distributions measured by Theus and collaborators (1955) *). Their results show differences with the results of the present experiments and with the calculated data of Goldstein and Wilkins. Consequently the discrepancies are also found in the buildup factors (see table IV). These discrepancies may be explained by the fact that these authors used a different analyzing method. Comparing the analyzing method used for the present measurements with the method used by Theus *et al*, the separated resolution cor-

*) There are reasons to believe that the results of Theus and collaborators (J. Appl. Phys. *26*, 294 (1955)) are represented with a factor 10 in error. In the representation in fig. VI–2 this error is eliminated. The given photon energy distributions (dashed lines) also were renormalized to a source strength of one photon per second.

rection and the correction for the multiple scattering within the crystal may be mentioned as the principal differences.

As for the resolution correction, there seems to be no mathematical proof, that the correction can be carried out by matrix inversion. To include the resolution correction in an overall correction matrix, as has been done by Theus and collaborators, therefore is quite dangerous. Also in the resolution correction used here, there is no proof for the validity of the matrix inversion method. The occurring 'oscillations' in the solution (see fig. IV–3) may be due to this mathematical difficulty. Iterative methods, as proposed by Freedman *et al* (1956), Villforth *et al* (1958) and Skarsgard *et al* (1961) entail the same difficulties. If, however, matrix inversion or an iterative procedure is combined with 'trial and error' calculations, the obtained results may fairly represent the true electron energy distributions in the crystal.

The escape correction can be carried out in an arbitrarily close approximation, provided that the kernel of the integral equation involved represents all factors concerning the escape effects in the crystal within reasonable accuracy. Neglecting multiple scatter effects in a crystal of the size as used in this work seems not to be justified, as may be apparent from fig. V–6. Therefore, the multiple scatter effects in the crystal were taken into account by experimental methods (see section V.8). In the analyzing method used by Theus and collaborators these effects were neglected for a crystal of 2.54 cm diameter and 1.27 cm thickness. As their results show large differences with calculated data, which is not the case with the present results, it is believed that the error made in this neglection must be quite large.

Summarizing it can be stated that measurements of continuous photon energy distributions with geometries similar to those encountered in practice, are possible with the aid of scintillation spectrometry, provided that the measurements are performed very carefully, that the measured pulse height spectra are interpretated properly and that possible simplifications are considered thoroughly.

CHAPTER VII

Possible experiments with different geometries

As long as a scattering medium can be considered as homogeneous and infinite, the calculations on photon energy distributions and buildup factors carried out by Goldstein and Wilkins (1954), which calculations extend over a long range of energies and scattering materials, are extremely valuable. In practice, however, very often situations are found which do not satisfy the conditions of homogeneity and infinity. Though in general a knowledge of the buildup factors is sufficient in practice, in some cases it might be important for understanding the buildup phenomena to know about scattered photon energy distributions. In most of these practical cases calculations are almost impossible, the only way to obtain such data, without direct measurements, being the performance of (expensive and time consuming) Monte Carlo computations. So measurements may be of great help in such situations.

As has been stated in chapter II it is meaningful to start with measurements of scattered photon energy distributions with simple geometries. Measurements in such a simple geometry have been described in that chapter. As, however, it has been proved in this work that measurements of continuous energy distributions are possible with an acceptable degree of accuracy, measurements can be carried out in a variety of geometries, although the physical interpretation of the results remains a problem that has still to be solved. Measurements can be carried out, for example, with geometries found in radiation dosimetry (measurements in phantoms representing the human body or parts of it). In such cases, however, the use of a very small detector is preferable. Since very small photomultipliers are not available, such measurements have to be carried out with a very small NaI/Tl crystal which is coupled to a lightpipe, which in turn is coupled to a photomultiplier outside the medium. Pulse height spectra, measured with such a detector, can be corrected according to the method described in the chapters III, IV and V, provided that a new escape matrix is constructed. This new matrix is probably much simpler than the matrix given in table VI, the occurrence of multiple interactions in a small crystal being unlikely. A disadvantage is the worsening of the resolution, due to light losses in the lightpipe.

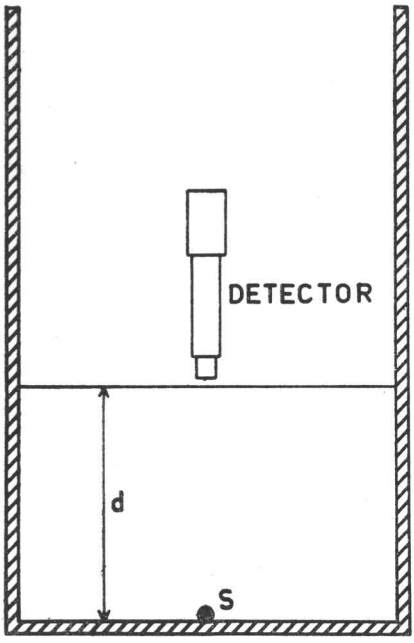

Fig. VII–1. Measuring set-up with a double interface geometry.

In dosimetry problems as well as in shielding problems the presence of interfaces between different materials may play an important role. Accordingly it may be sensible to measure photon energy distributions near interfaces, for example between tissue and air, tissue and bone (dosimetry), concrete and water, and iron and water (shielding).

An example of measurements with such an interface geometry is illustrated in fig. VII–1. The measurements with this geometry concern an investigation of a double interface problem: a point isotropic source is placed at one of the flat boundaries of a 'water disk', the detector immediately above the other flat boundary. The thickness of the water disk was respectively 1, 2 and 3 mean free path lengths in water of photons with an energy of 0.66 MeV (respectively 11.7 cm, 23.4 cm and 45.1 cm). The resulting scattered photon energy distributions are given in fig. VII–2. These results are obtained by applying the correction method, described in the chapters III, IV, and V. From these measured photon energy distri-

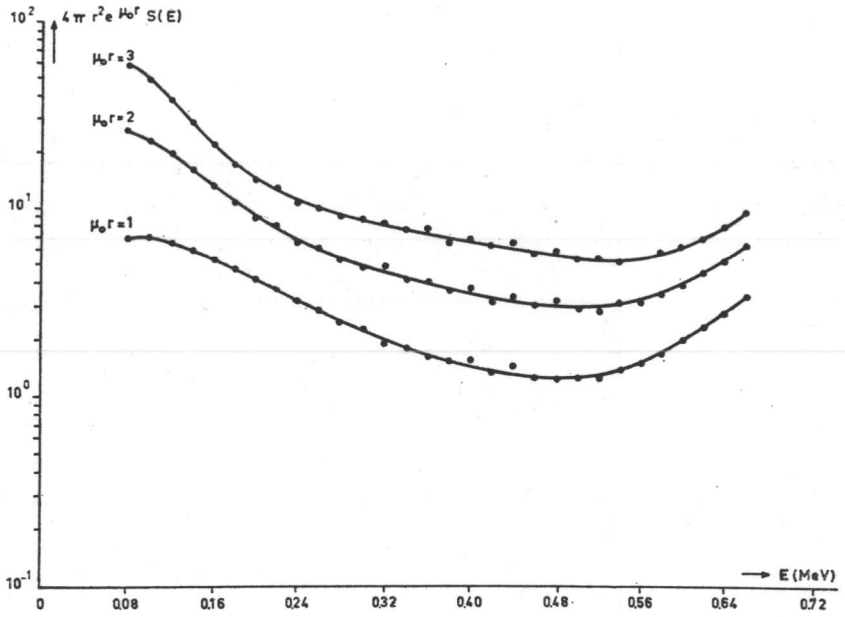

Fig. VII–2. Photon energy distributions at the interface water–air at three penetration distances, measured with a double interface geometry.

butions the energy buildup factors B_E, the energy absorption buildup factors B_a and the exposure dose buildup factors B_d are determined by integration (see section VI.2). The buildup factors are given in table V.

	$\mu_0 r = 1$	$\mu_0 r = 2$	$\mu_0 r = 3$
B_E	2.4	4.5	7.6
B_a	2.4	4.2	7.3
B_d	2.3	4.2	7.2

Table V. Energy buildup factors (B_E), energy absorption buildup factors (B_a), and exposure dose buildup factors (B_d) at three penetration distances with a double interface geometry.

A double interface geometry, such as described above may be found in shielding problems. This experiment, however, is given only as an example. In shielding problems also higher energies are involved. Accordingly experiments can be carried out with sources of higher photon energies if the escape matrix, as given in table VI, is extended to higher energy values.

Summary

In the applications of ionizing radiation in medicine, as well as in industrial and scientific application of intensive radioactive sources, gamma ray penetration problems are extremely important. These penetration problems, which in most cases concern bad geometry configurations, are characterized by multiple scatter phenomena in the penetrated medium. The discrepancy, existing between 'good geometry' calculations and measurements in 'bad geometry' configurations can be conveniently expressed in multiplicative factors, the so called buildup factors.

Several calculation methods of various degrees of rigour have been elaborated for finding data about energy distributions of multiple scattered gamma and X-radiation. The few known experimental data to check these calculations are not quite satisfactory. This is due to the fact that experimental determinations of energy distributions meet with difficulties.

In the work described in this thesis an attempt is made to overcome these difficulties. With the aid of a scintillation spectrometer pulse height distributions, resulting from the scattering of 0.66 MeV gamma rays of ^{137}Cs, were measured within a cylindrical bounded water medium at three different source–detector distances. The nuclide ^{137}Cs was chosen because of its monoenergetic gamma radiaton, the energy of which being comparable to energies involved in medical applications (if photons with different energies are emitted by the source, the correction of the measured pulse height spectra becomes more complicated). With such photons a reasonable buildup can be expected. The measuring geometry can be considered as a point isotropic source geometry (chapter II). The changes in the scattering pattern, caused by the displacement of the medium by the detector was found to be negligible (chapter II).

In order to derive the scattered photon energy distributions from the measured pulse height spectra, the response of the scintillation detector to an incident photon energy distribution was expressed in an integral equation. The kernel of this integral equation was analyzed (chapter III). While corrections for the escape effects in the scintillation crystal can be made without any difficulty, provided that the escape effects are quantitatively known, the sharpening of the spectrum, which is smeared out by spreading processes in the detector, is not easily done. For this reason the pulse height distribution correction is carried out in two steps.

The first step concerns the sharpening of the spectrum (the resolution correction). The integral equation, describing the smearing out of the spectrum, can be approximated by a matrix equation

$$\mathbf{h} = \mathbf{Ng}$$

in which **h** is the measured pulse height distribution, given as a set of numbers, **g** is the electron energy distribution within the crystal, generated by incident photons and also given numerically, and **N** is a matrix, constructed from a gaussian function in which the relative variance, being energy dependent, can be described with two parameters.

Since the 30 × 30 matrix used in this work is not in a good condition (chapter IV), simple matrix inversion gives rise to difficulties resulting in the occurrence of oscillations in the solution **g**. Also iterative procedures, such as proposed by Freedman *et al* (1956), Villforth *et al* (1958) and Skarsgard *et al* (1961), cannot be applied in a satisfactory way because of the bad condition of the matrix **N**. Nevertheless in this work matrix inversion was carried out, but it was coupled with a 'trial and error' calculation which yielded quite satisfactory results (chapter V).

The second step is the correction for the escape effects in the crystal. The integral equation involved, which is a Volterra equation, can be approximated by the matrix equation

$$\mathbf{g} = \mathbf{Ks}$$

in which **s** is the incident photon energy distribution and **K** is the escape matrix. The matrix **K**, being constructed from the kernel of a Volterra equation, is essentially triangular. Inversion can be carried out without any difficulty since none of the diagonal elements tends to become zero.

The escape matrix **K** is determined by several quantities which are discussed in chapter V. These quantities are:

a. the total efficiency, being defined as the probability of interaction of the incident photons. This quantity was evaluated by assuming the detector to be isotropic;
b. the photopeak efficiency, being defined as the ratio of the joint areas of the photopeak and the X-ray escape peak to the spectrum. This quantity was determined experimentally;
c. The X-ray escape probability, being defined as the ratio of the area of the X-ray escape peak to the photopeak. Axel (1953) has

offered approximating calculations of this quantity which calculations were used in this work;

d. the escape probability of the photons scattered in the crystal, which had to be determined experimentally because of the occurrence of multiple effects in the crystal. This was done with the aid of an interpolation carpet;
e. The backscatter probability, which quantity was also evaluated experimentally.

From these quantities the escape matrix **K** was calculated. This escape matrix and its inverse are given in table VI.

The described correction method was applied to the measured pulse height distributions. The resulting photon energy distributions for a bounded medium were compared with calculations according to the 'moment method' of Spencer and Fano (1951) for an infinite medium. To this purpose interpolations from the data of Goldstein and Wilkins (1954) were made. The experimental results agree with these calculations, in most cases within the measuring accuracy of 10% and maximal within 15%.

A comparison was also made with the experimental results of Theus *et al* (1955). Their experimental results deviate from the results of the present experiments, which deviation can be explained by the difference in the method used for analyzing the measured pulse height spectra.

From the experimental photon energy distributions the energy buildup factors, the energy absorption buildup factors and the exposure dose buildup factors were derived. Consequently these buildup factors agree with 'moment method' calculations.

These results can be considered as a mutual confirmation, both for the correctness of the measurements within the measuring accuracy and for the validity of the 'moment method' calculations in a geometry such as described. Hence it can be concluded that:

a. in the measuring set-up described the cylindrical water medium can be considered as an infinite medium for 0.66 MeV gamma rays, and
b. measurements of continuous photon energy distributions with geometries similar to those encountered in practice are possible with the aid of scintillation spectrometry, provided that the measurements are performed very carefully, that the measured pulse height spectra are properly interpretated, and that possible simplifications are considered thoroughly.

Samenvatting

Zowel in toepassingen van ioniserende straling in de geneeskunde als in het industriële en wetenschappelijke gebruik van sterke radioactieve bronnen is de doordringing van gammastraling een belangrijk probleem. Deze doordringing, in de meeste gevallen volgens een z.g. 'brede bundel-geometrie', gaat vergezeld van meervoudige-verstrooiïngsverschijnselen in het betreffende medium. De discrepantie die ten gevolge hiervan bestaat tussen berekeningen volgens de z.g. 'smalle bundel-geometrie' enerzijds en metingen in de 'brede bundel-geometrie' anderzijds, kan op geschikte wijze worden uitgedrukt in vermenigvuldigingsfactoren, de z.g. aangroei-factoren.

Verschillende min of meer exacte berekeningsmethoden zijn ontwikkeld om gegevens te verkrijgen omtrent de energieverdelingen van verstrooide gamma- en röntgenstraling. De schaarse experimentele gegevens voor de toetsing van deze berekeningen geven tot nu toe echter nog weinig bevredigende resultaten. Dit is het gevolg van het feit, dat metingen van energieverdelingen op moeilijkheden stuiten.

In het onderzoek, beschreven in deze dissertatie, is een poging aangewend om over deze moeilijkheden heen te komen. Met behulp van een scintillatie-spectrometer zijn de amplitudespectra, die uit de verstrooiïng van de monoënergetische gammastraling van ^{137}Cs (met een energie van 0,66 MeV) ontstaan, gemeten. Voor de proefopstelling is dit nuclide gekozen omdat het monoënergetische gammastraling uitzendt (wanneer de bron fotonen met verschillende energie uitzendt, wordt de correctie van de gemeten amplitudespectra ingewikkelder) met een energie die vergelijkbaar is met energieën die in medische toepassingen gebruikelijk zijn en waarmee een redelijke aangroei te verwachten is. De metingen werden in een cylindrisch begrensd watermedium uitgevoerd met drie verschillende afstanden tussen de detector en de bron. De geometrie kon worden beschouwd als een puntisotropische brongeometrie (hoofdstuk II). De veranderingen die als een gevolg van de verplaatsing van het medium door de detector in het verstrooiïngspatroon kunnen optreden, bleken verwaarloosd te kunnen worden (hoofdstuk II).

Om uit de gemeten amplitudespectra de energieverdelingen van de verstrooide fotonen te kunnen bepalen, is de responsie van de scintillatiedetector uitgedrukt in een integraalvergelijking. De kern van deze integraalvergelijking is nader onderzocht (hoofdstuk III). Uit dit onderzoek bleek

dat het corrigeren van de ontsnappingseffecten, die in het scintillatiekristal optreden, zonder mathematische moeilijkheden kan worden uitgevoerd. De grootheden die deze ontsnappingseffecten bepalen, moeten dan kwantitatief bekend kunnen zijn. Het spectrum is echter ten gevolge van processen die in de detector volgens bepaalde statistieken verlopen, 'uitgesmeerd'. Het wegwerken van deze 'uitsmering' stuit op moeilijkheden. Om deze reden is de correctie van de gemeten amplitudeverdelingen in twee stappen uitgevoerd: De eerste stap betreft het wegwerken van de 'uitsmering' in de gemeten amplitudespectra. De integraalvergelijking die dit 'uitsmeringsproces' beschrijft, kan worden benaderd door een matrixvergelijking:

$$\mathbf{h} = \mathbf{Ng}.$$

Hierin is **h** het gemeten amplitudespectrum, gegeven als een reeks van getallen, **g** de energieverdeling van de elektronen, die door de invallende fotonen in het kristal worden vrijgemaakt, eveneens gegeven als een reeks van getallen, en **N** een matrix die gevormd is uit een normale waarschijnlijkheidsfunctie, waarvan de energieafhankelijke relatieve variantie beschreven kan worden met behulp van een tweetal parameters.

De conditie van de 30×30 matrix, die in dit onderzoek werd toegepast, bleek niet goed te zijn (hoofdstuk IV), waardoor een eenvoudige matrix-inversie moeilijkheden opleverde, welke moeilijkheden zich manifesteerden in oscillaties in de oplossing **g**. Ten gevolge van de slechte conditie van de matrix **N** is ook de toepassing van iteratieve methoden, zoals die welke door Freedman et al (1956), door Villforth et al (1958) en door Skarsgard et al (1961) zijn voorgesteld, niet op bevredigende wijze mogelijk.

In dit onderzoek is toch een matrix-inversie toegepast, waaraan echter een 'trial and error'-berekening is toegevoegd. Hiermee zijn zeer bevredigende resultaten verkregen (hoofdstuk V).

De tweede stap is het corrigeren van de ontsnappingseffecten in het kristal. De betreffende integraalvergelijking is een Volterra vergelijking, die eveneens kan worden voorgesteld door een matrixvergelijking:

$$\mathbf{g} = \mathbf{Ks},$$

waarin **s** de energieverdeling van de invallende fotonen en **K** de z.g. ontsnappingsmatrix is. Aangezien de matrix **K** uit de kern van een Volterra

vergelijking is gevormd, is **K** een driehoeksmatrix waarvan de inversie geen enkele moeilijkheid oplevert, daar geen van de diagonaalelementen gelijk is aan 0.

De ontsnappingsmatrix **K** wordt bepaald door een aantal grootheden die in hoofdstuk V uitvoerig zijn besproken. Deze grootheden zijn:

a. Het totale rendement, dat gedefinieerd is als de waarschijnlijkheid dat een invallend foton in wisselwerking met de kristalmaterie gaat. Deze grootheid is berekend met de op metingen gebaseerde veronderstelling dat de detector als isotroop kan worden beschouwd.
b. Het rendement van de fotopiek, dat gedefinieerd is als de verhouding van de som van de oppervlakken van de fotopiek en de fluorescentie-vluchtpiek ten opzichte van het oppervlak van het gehele spectrum. Deze grootheid is experimenteel bepaald.
c. De ontsnappingskans van de fluorescentiestraling, die gedefinieerd is als de verhouding van het oppervlak van de fluorescentie-vluchtpiek ten opzichte van dat van de fotopiek.
In dit onderzoek zijn de benaderende berekeningen van Axel (1953) gebruikt voor de bepaling van deze grootheid.
d. De ontsnappingskans van de fotonen die in het kristal worden verstrooid. Deze ontsnappingskans moest experimenteel worden bepaald, daar meervoudige wisselwerkingen in het kristal een theoretische benadering onmogelijk maken. De waarden van deze grootheid zijn uiteindelijk verkregen met behulp van een interpolatie-netwerk.
e. De waarschijnlijkheid van terugstrooiïng tegen delen van de detector. Ook deze grootheid is experimenteel bepaald.

Met behulp van deze aldus bepaalde grootheden is de ontsnappingsmatrix **K** berekend. Deze ontsnappingsmatrix is tezamen met zijn inverse gegeven in tabel VI.

De beschreven correctiemethode is toegepast op de metingen van de amplitudespectra. De resulterende energieverdelingen van verstrooide fotonen (in begrensde media) zijn vergeleken met berekeningen gemaakt volgens de z.g. 'moment-methode' van Spencer en Fano (1951) (die gelden voor oneindige media). Hiertoe zijn gegevens van Goldstein en Wilkins (1954), die berekeningen volgens deze methode hebben uitgevoerd, op de hier beschouwde energie en doordringingsafstanden geinterpoleerd. De resultaten van de experimenten bleken meestal bin-

nen een meetnauwkeurigheid van 10% en binnen maximaal 15% overeen te komen met deze berekeningen.

De meetresultaten zijn ook vergeleken met die welke door Theus et al (1955) zijn verkregen. De meetresultaten van deze auteurs wijken af van die welke in deze dissertatie zijn beschreven. Deze afwijking kan worden verklaard uit het verschil in de methode, die voor het analyseren van de gemeten amplitudespectra is gebruikt.

Uit de experimenteel bepaalde energieverdelingen van de verstrooide fotonen zijn achtereenvolgens de 'energie-aangroeifactoren', de 'energie-absorptie-aangroei-factoren', en de 'bestralingsdosis-aangroei-factoren' bepaald. Zoals moet volgen uit de bovengenoemde overeenstemming, kwamen ook deze 'aangroeifactoren' binnen de meetnauwkeurigheid overeen met berekeningen volgens de 'moment-methode'.

Deze resultaten kunnen worden gezien als een wederkerige bevestiging, zowel voor de juistheid van de meetresultaten binnen de meetnauwkeurigheid, als voor de toepasbaarheid van berekeningen volgens de 'moment-methode' in een geometrie als is beschreven. Dus kan worden geconcludeerd dat

a. in een meetopstelling zoals is beschreven, een cylindrisch watermedium kan worden beschouwd als een oneindig medium voor gammastralen met een energie van 0,66 MeV, en dat
b. metingen van continue energieverdelingen van fotonen volgens de in de praktijk bekende geometrieën kunnen worden uitgevoerd met behulp van scintillatie-spectrometrie, vooropgesteld dat de metingen zeer zorgvuldig worden uitgevoerd, dat de gemeten amplitudespectra op de juiste wijze worden geïnterpreteerd en dat eventuele vereenvoudigingen grondig worden overwogen.

References

ADAMS, G. D., *Radiology 69*, 867 (1958)

AXEL, P., *BNL rep. 271* (1953)

BERGER, M. J., *J. Res. Nat. Bur. Stand. 55*, 343 (1955)

BERGER, M. J., *J. Res. Nat. Bur. Stand. 56*, 111 (1956)

BERGER, M. J., *J. Appl. Phys. 28*, 1502 (1957)

BERGER, M. J. AND SPENCER, L.V., *Radiat. Res. 10*, 552 (1959)

BERGER, M. J. AND RASO, D. J., *Radiat. Res. 12*, 20 (1960)

BISI, A. AND ZAPPA, L., *Nucl. Instr. 3*, 17 (1958)

BRUCE, W. R. AND JOHNS, H. E., *Brit. J. Rad. 28*, 443 (1955)

CORMACK, D. V., DAVITT, W. E., BURKE, D. G. AND RAWSON, E. G., *Brit. J. Rad. 31*, 565 (1958)

CORMACK, D. V. AND JOHNS, H. E., *Brit. J. Rad. 31*, 497 (1958)

COURANT, R. AND HILBERT, D., *Methoden der mathematischen Physik I, Verlag Jul. Springer, Berlin*, 96–137 (1931)

DIXON, W. R., *Can. J. Phys. 36*, (1958)

DIXON, W. R. AND AITKEN, J. H., *Can. J. Phys. 36*, 1624 (1958)

DROSTE, G. FHR VON, *Zeits. f. Phys. 100*, 529 (1936)

FANO, U., *Nucleon. 11*, 8 and 55 (1953)

FANO, U. AND NELMS, A., *J. Res. Nat. Bur. Stand. 59*, 207 (1957)

FINE, S. AND HENDEE, C. F., *Nucleon. 13*, (3), 36 (1955)

FOLDI, L., *Phys. Rev. 81*, 395 (1951)

FREEDMAN, M. S., NOVEY, T. B., PORTER, F. T. AND WAGNER Jr., F., *Rev. Sci. Instr. 27*, 716 (1956)

GARRET, O. AND WHYTE, G. M., *Phys. Rev. 95*, 889 (1954)

GOLDSTEIN, H. AND WILKINS, J. E., *Rep. NDA–15C–41*, Oak Ridge (1954)

HAYWARD, E., *Phys. Rev. 86*, 493 (1953)

HEITLER, W., '*The Quantum Theory of Radiation*', 3rd ed. Oxford Clarendon Press (1954)

HOFSTADTER, R., *Phys. Rev. 74*, 100 (1948)

JAEGER, R. AND KOLB, W., *Strahlentherapie 104*, 29 (1957)

KALLMANN, H. AND DRESNER, *Phys. Rev. 114*, 71 (1959)

KELLEY, G. G., BELL, P. R., DAVIS, R. C. AND LAZAR, N. H., *Nucleon. 14*, (4), 53 (1956)

KROKOWSKI, E., *Strahlentherapie 104*, 442 (1957)

LAMERTON, L. F., *Brit. J. Rad. 21*, 276 and 352 (1958)

LAZAR, N. H., DAVIS, R. C. AND BELL, P. R., *Nucleon. 14* (4), 52 (1956)

LIDÉN, K. AND STARFELT, N., *Arkiv f. Fys. 7*, 427 (1954)

LOEVINGER, R., JAPHA, E. M. AND BROWNELL, G. L., *Radiation Dosimetry* (Hine and Brownell), Acad. Press Inc. (1956)

MAEDER, D., MULLER, R. AND WINTERSTEIGER, V., *Helv. Phys. Acta 27*, 3 (1954)

MAIGNAN, P., *An. Phys. 8*, 202 (1953)

MAYNEORD, W. F. AND LAMERTON, L. F., *Brit. J. Rad. 14*, 255 (1941)

MAYNEORD, W. F., '*Some Applications of Nuclear Physics to Medicine*' *Brit J. Rad.* Suppl. 2 (1950)

MELLINK, J. H., *Act. Rad. 42*, 305 (1954)

MELLINK, J. H., *J. Belge Rad. 40*, 544 (1957)

MORGAN, R. H., *Handbook of Radiology*, Year Book Publ. Inc. Chicago, (1955)

Tables of Normal Probability Functions, Nat. Bur. Stand. Appl. Math. Series 23, (June 1953)

Table of Natural Logarithms, Nat. Bur. Stand. Appl. Math. Series 31, (October 1953)

PAYNE-SCOTT, R., *Brit. J. Rad. 10*, 850 (1937)

PARMENTIER, J. H., *Rapport Centr. Lab. T.N.O.* No. CL 60/34 (1960)

PEEBLES, G. H., *J. Appl. Phys. 24*, 1272 (1953)

PEEBLES, G. H., *J. Appl. Phys. 24*, 1437 (1953)

PERKINS, J. F., *J. Appl. Phys. 26*, 1372 (1955)

PERKINS, J. F., *J. Appl. Phys. 26*, 655 (1955)

PRICE, B. T. AND HORTON, C. C., *Radiation Shielding*, Pegam. Press (1957)

RAM, W. J., '*Radiation Dosimetry*' (Hine and Brownell), Acad. Press. Inc., 246 (1956)

RAWSON, E. G. AND CORMACK, D. V., *Nucleon. 16* (10), 92 (1958)

RICCI, R. A., *Physica 24*, 298 (1958)

O'ROURKE, R. C., *Phys. Rev. 85*, 881 (1952)

O'ROURKE, R. C., *Phys. Rev. 89*, 999 (1953)

SKARSGARD, L. D. AND JOHNS, H. E., *Radiat. Res. 14*, 231 (1961)

SKARSGARD, L. D., JOHNS, H. E. AND GREEN, L. E. S., *Radiat. Res. 14*, 261 (1961)

SCHAAL, A., *Fortschr. Roentgenstr. 88*, 475 (1958)

SOOLE, B. W., *Proc. Phys. Soc.* (London) A*230*, 343 (1955)

SPENCER, L. V. AND FANO, U., *J. Res. Nat. Bur. Stand. 46*, 466 (1951)

TAYLOR, C. J., JENTSCHKE, W. K., REMLEY, M. E., EBY, F. S. AND KRUGER, P. G, *Phys. Rev. 84*, 1034 (1951)

THEUS, R. B., BEACH, L. A. AND FAUST, W. R., *J. Appl. Phys. 26*, 294 (1955)

THORAEUS, R., *Acta Radiol.*, Stockholm *51*, 473 (1959)

VILLFORTH, J. C., BIRKHOFF, R. D. AND HUBBELL Jr, H. H., *ORNL rep.* 2529 (1958)

DE WAARD, H., *Ned. Tijdschr. v. Nat. 21*, 1 and 33 (1955)

DE WAARD, R., *Proc. Kon. Ned. Acad. Wetensch. 49*, 855 (1946)

WAPSTRA, A. H., *Diss.* Amsterdam (1953)

WAPSTRA, A. H., '*Nuclear Spectroscopy Tables*', North Holland Publ. Cie, Amsterdam (1959)

WHITTAKER, E. T. AND WATSON, G. N., *A Course of Modern Analysis 4th ed.*, Repr. Cambr. Univ. Press 211–231 (1958)

WHITE, G. R., *Phys. Rev. 80*, 154 (1950)

WHYTE, G. N., *Can. J. Phys. 33*, 96 (1955)

WIGNER, E. P., *Phys. Rev. 94*, 17 (1954)

YATES, H., '*Carpets and Lattices*', Aircraft Eng. Jan. 1946, 8

Center of Photon Energy Interval (MeV)	Energy corresponding to Center of Pulse Height Inte						
	0.08	0.10	0.12	0.14	0.16	0.18	0.20
0.08	7960						
0.10	475	8008					
0.12	216	325	8342				
0.14	0	139	209	7751			
0.16	0	0	85	127	7050		
0.18	0	0	0	50	74	6207	
0.20	0	0	0	0	21	32	537
0.22	15	0	0	0	0	9	1
0.24	77	63	49	0	0	0	
0.26	117	97	91	39	45	0	
0.28	145	127	115	91	121	12	
0.30	174	150	133	129	178	64	
0.32	181	163	144	131	167	180	3
0.34	184	165	160	168	179	191	6
0.36	181	169	161	164	167	181	8
0.38	177	167	157	153	165	174	8
0.40	173	162	153	148	156	167	16
0.42	170	160	151	143	142	146	14
0.44	157	149	142	136	134	146	14
0.46	153	146	139	134	131	138	14
0.48	147	140	135	129	125	128	13
0.50	144	136	129	123	118	128	13
0.52	136	128	122	117	114	117	13
0.54	127	120	115	111	108	108	12
0.56	118	113	108	104	100	99	11
0.58	113	109	106	103	101	100	11
0.60	107	104	101	97	96	97	11
0.62	102	99	96	93	92	96	11
0.64	97	95	92	90	92	97	11
0.66	93	91	89	87	91	97	11

rval (MeV)

0	0.22	0.24	0.26	0.28	0.30	0.32	0.34	0.36	0.38	0.40	0.42	0.4
5												
3	4578											
3	5	3931										
0	0	0	3380									
0	0	0	0	2899								
0	0	0	0	0	2477							
0	0	0	0	0	0	2140						
5	20	0	0	0	0	0	1879					
0	41	20	7	1	0	0	0	1679				
4	38	18	6	1	0	0	0	0	1501			
3	170	124	61	21	6	0	0	0	0	1349		
2	144	151	126	31	26	8	4	0	0	0	1208	
7	144	149	140	73	39	21	10	2	0	0	0	110
3	149	140	130	95	66	47	34	24	16	9	3	
9	142	131	129	105	79	61	46	33	22	14	7	
3	134	119	119	123	124	98	62	46	35	25	17	1
1	134	117	112	114	121	122	93	67	50	35	25	1
1	127	111	105	109	116	117	104	84	67	51	38	2
4	122	108	100	101	106	112	111	93	72	57	44	3
3	123	106	95	92	95	99	106	110	99	79	60	4
1	121	93	92	86	86	89	94	102	107	91	73	5
1	117	99	87	81	80	80	81	83	89	97	102	8
5	115	96	86	80	78	79	81	85	89	94	98	9
3	116	94	83	80	77	78	79	81	84	89	92	9

Table VIa. ESCAPE MATRIX

Multiply tabulated values by 10^{-4}

4	0.46	0.48	0.50	0.52	0.54	0.56	0.58	0.60	0.62	0.64	0.66
3											
0	1020										
2	0	954									
	5	0	892								
7	12	6	0	835							
3	19	11	5	0	775						
2	24	16	10	4	0	734					
5	30	21	13	7	3	1	684				
0	41	30	20	12	7	2	0	654			
5	56	38	25	15	8	3	1	0	619		
0	70	45	30	19	11	6	3	1	0	588	
2	86	61	41	25	17	11	7	3	1	0	560

Energy corresponding to Center of Pulse Height Interval (MeV)	Center of Photon Energy Interval (MeV)						
	0.08	0.10	0.12	0.14	0.16	0.18	0.20
0.08	+12563						
0.10	−950	+12487					
0.12	−281	−487	+12013				
0.14	+70	−181	−272	+12900			
0.16	+3	+17	−102	−152	+14185		
0.18	−1	+2	+6	−65	−104	+16113	
0.20	0	−3	+1	+5	−29	−48	+18605
0.22	−32	0	0	0	0	−14	−23
0.24	−155	0	0	0	0	0	−6
0.26	−267	−201	−182	−75	−92	0	0
0.28	−382	−304	−257	−202	−289	−30	0
0.30	−543	−422	−344	−334	−496	−187	0
0.32	−657	−540	−442	−349	−535	−615	−110
0.34	−785	−633	−573	−603	−673	−765	−281
0.36	−890	−757	−674	−689	−731	−843	−402
0.38	−1000	−864	−759	−738	−832	−933	−486
0.40	−1091	−937	−830	−808	−882	−1004	−1099
0.42	−1187	−1029	−913	−878	−895	−988	−1050
0.44	−1158	−1016	−913	−891	−894	−1062	−1181
0.46	−1160	−1030	−926	−911	−896	−1038	−1276
0.48	−1179	−1045	−958	−934	−902	−1019	−1300
0.50	−1149	−1013	−913	−886	−824	−1025	−1303
0.52	−1063	−935	−850	−832	−778	−901	−1333
0.54	−946	−840	−773	−765	−702	−781	−1236
0.56	−869	−799	−733	−724	−641	−696	−1216
0.58	−758	−715	−685	−688	−625	−665	−1204
0.60	−645	−633	−610	−597	−546	−600	−1163
0.62	−537	−536	−521	−526	−476	−569	−1138
0.64	−408	−443	−434	−454	−456	−564	−1216
0.66	−289	−338	−357	−377	−423	−549	−1277

0.22	0.24	0.26	0.28	0.30	0.32	0.34	0.36	0.38	0.40	0.42	0.44	0.46
+21842												
−11	+25445											
0	0	+29588										
0	0	0	+34493									
0	0	0	0	+40358								
0	0	0	0	0	+46730							
−93	0	0	0	0	0	+53218						
−223	−124	−49	−8	0	0	0	+59566					
−238	−129	−49	−9	0	0	0	0	+66637				
−1209	−1010	−565	−227	−76	0	0	0	0	+74144			
−1158	−1394	−1323	−379	−374	−135	−79	0	0	0	+82795		
−1259	−1496	−1599	−971	−610	−386	−216	−50	0	0	0	+90230	
−1412	−1529	−1621	−1383	−1131	−948	−806	−664	−510	−326	−123	0	+98039
−1468	−1563	−1763	−1681	−1490	−1355	−1202	−1006	−773	−560	−317	−98	0
−1464	−1502	−1733	−2127	−2536	−2363	−1758	−1525	−1336	−1087	−838	−590	−294
−1544	−1560	−1730	−2120	−2676	−3195	−2867	−2414	−2076	−1655	−1342	−994	−770
−1497	−1517	−1678	−2147	−2740	−3290	−3456	−3268	−3007	−2609	−2208	−1773	−1321
−1526	−1571	−1703	−2147	−2717	−3441	−4051	−3979	−3554	−3211	−2818	−2235	−1842
−1576	−1571	−1658	−2066	−2602	−3281	−4210	−5163	−5376	−4897	−4227	−3458	−2531
−1547	−1298	−1589	−1963	−2421	−3076	−3941	−5107	−6245	−6077	−5550	−4648	−3741
−1445	−1359	−1404	−1861	−2317	−2895	−3601	−4449	−5611	−7069	−8512	−7841	−5605
−1412	−1282	−1363	−1845	−2289	−2936	−3744	−4785	−5920	−7259	−8702	−9352	−7495
−1424	−1201	−1229	−1809	−2229	−2906	−3721	−4706	−5838	−7267	−8708	−9612	−9939

0.48	0.50	0.52	0.54	0.56	0.58	0.60	0.62	0.64	0.66

Table VIb. INVERTED ESCAPE MATRIX

Multiply tabulated values by 10^{-4}

+104783									
0	+112101								
−424	0	+119707							
−844	−418	0	+129025						
−1356	−924	−403	0	+136194					
−1958	−1323	−778	−362	−133	+146237				
−3028	−2205	−1446	−915	−289	0	+152895			
−4203	−3021	−1981	−1147	−476	−175	0	+161472		
−5322	−3877	−2686	−1689	−1021	−563	−204	0	+170124	
−7798	−5730	−3824	−2829	−2030	−1427	−663	−242	0	+178487

STELLINGEN

I

Iterative methoden als toegepast door Skarsgard en medewerkers, voor het oplossen van continue energiespectra uit de met behulp van scintillatiespectrometrie verkregen amplitudespectra, stuiten op dezelfde moeilijkheden als welke optreden bij een directe matrixinversie, wanneer de betreffende matrix in een slechte conditie verkeert.

L. D. SKARSGARD, H. E. JOHNS en L. E. S. GREEN,
Radiat. Res. *14*, 261 (1961).
Hoofdstuk III van dit proefschrift.

II

Volgens Kochenburger worden in niet-lineaire teruggekoppelde regelsystemen met periodieke ingangssignalen de hogere harmonischen, die achter het niet-lineaire deel ontstaan, door het lineaire deel uitgezeefd. Het is echter van belang na te gaan of de terugkoppeling zelf al niet een zodanige reductie van de hogere harmonischen kan geven, dat aan het lineaire deel minder eisen gesteld behoeven te worden.

R. J. KOCHENBURGER,
AIEE transactions *69*, 270 (1950).

III

Voor de transmissie van kiescijfers over grote afstanden in de automatische telefonie verdient het systeem van multitooncodering de voorkeur boven het systeem van toonfrequente impulscodering.

C. A. DAHLBLOM, A. W. HORTON Jr. en D. L. MOODY,
AIEE transactions *68*, 392 (1949).

IV

Bij het toetsen van de beeldkwaliteit in de televisie-opnameapparatuur dient meer aandacht geschonken te worden aan de weergave van bewegende beeldfragmenten.

V

Het verdient aanbeveling om een onderzoek in te stellen naar de mogelijkheid voor toepassingen van halfgeleiders als detectoren in de gammaspectrometrie.

VI

Bij het onderzoek naar omzettingen, bijvoorbeeld in biologische systemen, met behulp van gemerkte stoffen, kan uit metingen van het verloop van de gemerkte stof vaak een model worden afgeleid, dat uit een aantal enkelvoudige componenten bestaat. Het is dan echter beter uit te gaan van een reeds opgesteld model dat aan de metingen kan worden getoetst, dan om uit de metingen een zodanig aantal componenten af te leiden, dat de fysische, c.q. fysiologische interpretatie van het model een verwrongen karakter krijgt.

C. G. LEWALLEN, M. BERMAN en J. E. RALL,
J. Clin. Invest. *38*, 66 (1959).

M. BERMAN en R. SCHOENVELD,
J. Appl. Phys. *27*, 1361 (1956).

VII

In het model voor de synthese van eiwitten, dat door Rittenberg en San Pietro is voorgesteld, wordt de verstoring van het dynamisch evenwicht door het inbrengen van het gemerkte aminozuur ten onrechte verwaarloosd.

D. RITTENBERG en A. SAN PIETRO,
J. Biol. Chem. *201*, 457 (1953).

K. OLESEN, N. C. S. HEILSKOV en F. SCHØNHEYDER,
Biochem. Biophys. Acta *15*, 95 (1954)

VIII

De door Stein gemaakte schatting van de negatieve-entropievermeerdering bij de biologische celdeling berust op een aantal onjuiste veronderstellingen.

W. STEIN,
Naturwissensch. *47*, 542 (1960).

IX

Het aan patiënten meten van de opname van radioactief jodium in de schildklier heeft geen fysiologische en weinig diagnostische waarde tenzij de meetopstelling voldoet aan zeer stringente eisen betreffende de collimatie, de discriminatie van de verstrooide en teruggestrooide fotonen, de vergelijkingsstandaard en de afscherming.

X

Het verdient aanbeveling vaardigheid in het toepassen van interpolatie-netwerken bij het uitwerken van experimentele gegevens als een der eisen te stellen voor de propaedeutische examens aan de Technische Hogescholen.

XI

Aangezien een stralenbeschermingsdienst van een kernreactorinstituut zich in hoofdzaak gesteld ziet voor problemen die van preventief-technische aard zijn, is het beginsel dat aan het hoofd van een dergelijke dienst een medicus moet staan, in het algemeen niet gerechtvaardigd.

XII

Het gedragspatroon van een volk, bijvoorbeeld dat van het Indonesische volk met betrekking tot zijn nationalisme, kan pas worden begrepen als men zijn mythen kent.